



1 **Source apportionment and ecotoxicity of particulate pollution events**
2 **in a Major Southern Hemisphere Megacity: influence of biomass**
3 **burning and a biofuel impacted fleet**

4 Guilherme Martins Pereira^{1,2}, Leonardo Yoshiaki Kamigauti¹, Rubens Fabio Pereira¹, Djacinto Monteiro
5 dos Santos³, Thayná da Silva Santos², José Vinicius Martins⁴, Célia Alves⁵, Cátia Gonçalves^{5,a}, Ismael
6 Casotti Rienda⁵, Nora Kováts⁶, Thiago Nogueira⁷, Luciana Rizzo³, Paulo Artaxo³, Regina Maura de
7 Miranda⁸, Marcia Akemi Yamasoe¹, Edmilson Dias de Freitas¹, Pérola de Castro Vasconcellos², Maria
8 de Fatima Andrade¹

9 ¹Department of Atmospheric Sciences, Institute of Astronomy, Geophysics and Atmospheric Sciences, University of São
10 Paulo, 05508-090, São Paulo, Brazil.

11 ²Department of Chemistry, Institute of Chemistry, University of São Paulo, 05508-000, São Paulo, Brazil.

12 ³Department of Applied Physics, Institute of Physics, University of São Paulo, 05508-090, São Paulo, Brazil.

13 ⁴Department of Mineralogy and Geotectonics, Institute of Geosciences, University of São Paulo, 05508-080, São Paulo, Brazil.

14 ⁵Center for Environmental and Marine Studies, Department of Environment and Planning, University of Aveiro, 3810-193
15 Aveiro, Portugal

16 ⁶Center of Natural Environmental Sciences, University of Pannonia, Egyetem str. 10, 8200 Veszprém, Hungary

17 ⁷Department of Environmental Health, School of Public Health, University of São Paulo, 01246-904, São Paulo, Brazil.

18 ⁸School of Arts, Sciences and Humanities, University of São Paulo, 03828-000, São Paulo, Brazil.

19 ^aCurrent address: Department of Physics, University of León, Campus de Vegazana, 24071 León, Spain.

20 *Correspondence to:* Guilherme Martins Pereira (guilherme.martins.pereira@usp.br)

21 **Abstract.** The Metropolitan Area of São Paulo (MASP) in Brazil has reduced its vehicular emissions in the last decades.
22 However, it is still affected by air pollution events, mainly in the winter, characterized as a dry season. The chemical
23 composition of fine particulate matter (PM_{2.5}) was studied in the MASP during a 100-day dry period in 2019. PM_{2.5} samples
24 underwent an extensive chemical characterization (including inorganic and organic species), and submicrometer particle
25 number size distributions were simultaneously monitored. PM_{2.5} concentrations exceeded the new World Health
26 Organization's daily guidelines on 75% of sampling days, emphasizing the need for strengthening local regulations. Source
27 apportionment (Positive Matrix Factorization, PMF5.0) was performed, and the sources related to vehicular emissions remain
28 dominant (over 60% of PM_{2.5}). A high contribution of biomass burning was observed, reaching 25% of PM_{2.5} mass and
29 correlated with sample ecotoxicity. This input was associated with north and northwest winds, suggesting other emerging
30 sources besides sugarcane burning (forest fires and sugarcane bagasse power plants). A mixed factor of road dust and vehicular
31 emissions increased throughout the campaign was related to stronger winds, suggesting a significant resuspension. The sulfate
32 secondary formation was related to humid conditions. Additionally, monitoring size particle distribution allowed the
33 observation of particle growth on days impacted by secondary formation. The results pointed out that control measures of high



34 PM_{2.5} events should include the control of emerging biomass burning sources in addition to stricter rules concerning vehicular
35 emissions.

36 1 Introduction

37 According to the World Health Organization (WHO), a large part of the world's population lives in places where the
38 recommended air quality standards are not achieved, and this includes the Metropolitan Area of São Paulo (MASP), Brazil
39 (WHO, 2021; CETESB 2023), where thousands of tons of pollutants are released into the atmosphere every year. Natural and
40 anthropogenic sources produce atmospheric pollutants. The MASP has more than 21 million inhabitants and around 7 million
41 vehicles. In 2022, in the MASP, vehicles were responsible for 96% of CO emissions, 70% of HC, 60% of NO_x, 8% of SO₂,
42 and 37% of fine mode PM (CETESB, 2023). Among the pollutants, particulate matter is extensively studied, as it harms human
43 health and is associated with cardiovascular diseases and cancer (Cohen et al., 2017). Furthermore, particulate matter has
44 climatic effects, through the absorption and scattering of solar radiation and indirectly by affecting cloud microphysics (Li et
45 al., 2022; Pöschl, 2005).

46 Particles are emitted by different natural sources, such as volcanic eruptions, resuspension, and erosion of soils and
47 vegetation, while the dominant anthropogenic sources are vehicles, industrial activities, and biomass burning. The formation
48 of secondary particles is quite significant in some cities, such as São Paulo, where sulfate and nitrate concentrations are high
49 and secondary particles comprise half of the fine mode PM mass (Andrade et al., 2012; CETESB et al., 2023). Particulate
50 matter is a complex mixture, including inorganic species (water-soluble ions and element oxides) and carbonaceous species,
51 such as elemental carbon (EC, associated with soot), and organic carbon (OC) associated with organic compounds, some of
52 them with toxic properties, such as polycyclic aromatic hydrocarbons (PAHs) (Ravindra et al., 2008; Pöschl, 2005). The fine
53 fraction of particulate matter (PM_{2.5}) includes particles with aerodynamic diameters equal or lower than 2.5 μm that can
54 penetrate the respiratory system, reaching the alveoli. Smaller particles than 100 nm are called ultrafine particles and can reach
55 other organs through the lung vasculature (Schraufnagel, 2020; Kumar et al., 2014).

56 The vehicle fuel profile in the MASP is unique compared to other metropolises worldwide, with a significant proportion
57 of biofuels, especially in light duty vehicles (Andrade et al., 2017). The fleet has been running in gasoline and bioethanol
58 blends (gasohol, 73% of gasoline, 27%, ethanol), hydrated ethanol (5% of water), diesel and biodiesel blends (9% of biodiesel
59 produced from soybean) (Pereira et al., 2023a,b). The peak levels of ethanol use were reached at the end of 2018 and were
60 comparable to those of gasohol (Pereira et al., 2023a). Despite the exponential increase in the vehicle fleet since the 1980's,
61 particulate pollutants have been reduced in the last decades (Andrade et al., 2017). Sugarcane biomass burning in the
62 countryside also has been reduced due to control measures (Valente and Laurini, 2021). In addition to the large quantity of
63 pollutants generated locally, increasing events of transport of biomass burning from the Amazon and Central parts of Brazil
64 have been observed in the MASP at the end of the decade (Pereira et al., 2021; Miranda et al., 2017), occurring mainly in the
65 dry period (July-October) (Vieira et al., 2023). In 2014 and 2015, biomass-burning sources were apportioned and found to
66 explain nearly one-fourth of particulate matter in the dry season (Pereira et al., 2017b; Emygdio et al., 2018). Local biomass
67 burning was also relevant, including the burning of charcoal and wood in barbecue and pizzerias and waste burning (Kumar
68 et al., 2016). In the eastern region of the city, an area with high population density, roads with heavy vehicle traffic, highly
69 sealed, and many industries, the contribution in 2019 was 9.9% light vehicles, 42% heavy vehicles, and 47.3% soil dust and
70 local sources such as waste burning and industries (Vieira et al., 2023). A rise in the contribution of non-exhaust sources is
71 expected in the next few years due to control measures focused on vehicle exhaust.

72 The São Paulo State Environmental Company (CETESB) monitors legislated pollutants at 26 air quality stations
73 throughout the MASP. Despite the efforts of local governments to improve air quality in the region, in 2019, they all recorded
74 concentrations of PM_{2.5} above the value recommended by the WHO, reaching critical levels in the drier months (April to
75 September). Considering the aspects mentioned before, it is crucial to periodically update the chemical characterization of



76 particulate matter since Brazilian environmental agencies do not carry out such extensive monitoring. It can be said that particle
77 sources in São Paulo always need to be studied and identified, but this depends on good quality chemical composition data.
78 The composition of aerosols varies with the changing fleet and the policies concerning the burning of biomass, furthermore,
79 they are also influenced by the changing climate and meteorological conditions. In recent years, dryer weather conditions in
80 the winter have favored forest and crop fires in central Brazil and the accumulation of pollutants (Souto-Oliveira et al., 2023;
81 Pereira et al., 2021). This study aims to thoroughly characterize PM_{2.5} chemical composition and toxicity in the MASP,
82 identifying the relative contribution of emission sources. Associations with weather conditions and case studies of air pollution
83 events were also investigated. The adoption of receptor models was performed to study the emission sources of PM_{2.5}, and
84 these results were associated with particle size distributions.

85 2 Materials and methods

86 2.1 Sampling of PM_{2.5} and particle number size distributions monitoring

87 High-volume samplers (Energética, Brazil) (1.13 m³ min⁻¹ flow) were employed to collect PM_{2.5} on the rooftop of the Institute
88 of Chemistry building at the University of São Paulo, in the city of São Paulo, Brazil (23°33'53"S, 46°43'32"W), located in a
89 green area, and more than 2 km away from a busy expressway (Marginal Pinheiros) (Figure 1). The sampling extended between
90 June 04 and September 12, 2019, in a pre-lockdown polluted period, starting six months before the pandemic. Ninety-nine
91 samples were collected for 24 hours (starting at 9 AM, local time). Quartz fiber filters (20 cm × 25 cm, Whatman, UK) were
92 employed to collect PM_{2.5}. These filters were decontaminated before sampling by heating at 600 °C for 6 h. Before and after
93 sampling, the filters were weighed in a microbalance (controlled temperature and humidity for equilibrium: T = 25 °C and RH
94 = 50%). Then, the filters were wrapped into a laminated sheet and stored at 5 °C to avoid volatilization and reactions of the
95 analytes before the analysis (de Oliveira Alves et al., 2015; Souza et al., 2014).



96

97 **Figure 1:** Sampling site location (marked in red) (© Google Maps).

98 Particle number size distributions (PNSD) were monitored using a Scanning Mobility Particle Sizer (SMPS 3081, TSI
99 Inc) in association with a Condensation Particle Counter (CPC 3010, TSI Inc). The system provided particle number size
100 distributions in the size range from 10 to 450 nm every 2 min. PNSD measurements were averaged to match the filter sampling
101 periods. Average distributions were also calculated for periods of interest in the dataset. The SMPS data were collected on the
102 rooftop of the Institute of Astronomy, Geophysics, and Atmospheric Sciences of the University of São Paulo, 500 meters from
103 the Institute of Chemistry. The data collection campaign took place at non-consecutive intervals from June 2019 to January
104 2020, totalizing 152 sampling days.



105 2.2 Analytical procedures

106 Distinct chemical composition analyses were performed, thus, pieces of the filters were sent to each laboratory. At the Institute
107 of Chemistry (University of São Paulo), water-soluble ions (WSI) and PAHs were determined. The extraction of WSI from
108 filters (4 cm²) was performed with 10 mL of deionized water (Milli-Q, Merck Millipore, USA) under sonication for 15 min.
109 Then, extracts were filtered with syringe filters (Millex-GV, 0.22 μm, PVDF), and cations and anions were quantified in an
110 ion chromatograph (Modules 819, 830, 833, 818, and 820, Metrohm, Switzerland). Anions F⁻, Cl⁻, NO₂⁻, Br⁻, NO₃⁻, PO₄³⁻,
111 SO₄²⁻, C₂O₄²⁻, HCO₂⁻, and C₄H₂O₄²⁻, and cations Ca²⁺, Mg²⁺, K⁺, NH₄⁺, and Na⁺ were quantified. Pereira et al. (2023a) describe
112 the adopted columns and eluents. Fluka (Switzerland) analyte standards were used. Recoveries fell between 80-120% and were
113 obtained by adding known concentrations of standards to blank filters and are reported in Table S1.

114 Punches of approximately 20 cm² from the filters underwent extraction using ultrasonic baths with 80 mL of
115 dichloromethane for three cycles of twenty minutes, as described by Pereira et al. (2017a). The extracts were concentrated via
116 rotary evaporation under low pressure (at 35°C for approximately 30 minutes) and fractionated on a chromatographic column
117 packed with 1.5 g silica gel. The methodology described in Vasconcellos et al. (2010) was modified and adopted in this study,
118 involving three elutions: the first carrying alkanes (10 mL of hexane), the second (9.6 mL of hexane + 5.4 mL of toluene), and
119 the third (7.5 mL of hexane and 7.5 mL of dichloromethane) carrying PAHs and their derivatives. The second and third
120 fractions were combined to enhance recovery. The fractionated extracts were concentrated by rotary evaporation under reduced
121 pressure (at 35°C for approximately 15 minutes), filtered, stored in 2 mL vials, dried, and reconstituted with 0.5 μL of hexane.
122 Samples were diluted prior to analysis by gas chromatography coupled with mass spectrometry (GC/MS, Agilent, GC 7820A,
123 and MS 5975), using an Agilent VF-5ms column (stationary phase, 30 m × 0.250 mm × 0.25 μm), with helium as the carrier
124 gas (99.97% purity and flow rate of 1.0 mL min⁻¹). The following species were determined: phenanthrene (Phe), anthracene
125 (Ant), fluoranthene (Flt), pyrene (Pyr), retene (Ret), benzo(a)anthracene (BaA), chrysene (Chr), benzo(b)fluoranthene (BbF),
126 benzo(k)fluoranthene (BkF), benzo(e)pyrene (BeP), benzo(a)pyrene (BaP), indene(1,2,3-c,d)pyrene (InP),
127 dibenzo(a,h)anthracene (DBA) and benzo(g,h,i)pyrene (BPe) and coronene (Cor). Recovery was assessed by adding known
128 quantities of PAHs mix to filters containing 15 mg of the certified material (Urban Dust SRM 1649b, NIST, USA). Most
129 species presented values between 80 and 120%, averaging 100% (Table S1).

130 Carbonaceous species (OC and EC) in the quartz fiber filters were determined through thermal-optical analysis using a
131 *Sunset Laboratory Inc.* carbon analyzer at the Institute of Physics of the University of São Paulo. The EUSAAR-2 temperature
132 protocol (Cavalli et al., 2010) was employed, and the transmittance-based pyrolysis correction was applied, similar to previous
133 studies conducted in the MASP (Monteiro dos Santos et al., 2016). Temperature-resolved carbon fractions are obtained, with
134 increasing temperatures: four for organic fractions (OC1 to OC4, from higher to lower volatility temperatures), four for
135 elemental carbon (EC1 to EC4), and the organic pyrolyzed carbon (PC) is monitored. Total OC is the sum of OC1, OC2, OC3,
136 OC4, and PC, while total EC is the sum of EC1, EC2, EC3, and EC4, subtracted by PC. Secondary organic carbon (SOC) was
137 estimated considering the 5th percentile of the OC/EC ratios, similar as in Monteiro dos Santos et al. (2016). Organic matter
138 (OM) was calculated as 1.6 × OC, as adopted for urban aerosols (Turpin and Lim, 2001).

139 Quartz fiber filters were subjected to acid digestion using a microwave digester oven (CEM MDS-2000, USA) at the
140 Institute of Geosciences of the University of São Paulo. A strip of 20 cm × 2.5 cm of the filter was submitted to digestion in a
141 closed vessel (PFA) with a mixture of HNO₃ and H₂O (10 and 15 mL, respectively), then the volume was adjusted to 50 mL.
142 Major and trace elements were quantified by inductively coupled plasma mass spectroscopy (ICP-MS, model iCAP Q, Thermo
143 Fisher Scientific, USA). The percent recoveries and detection limits were previously reported for all the determined analytes
144 and reported in Pereira et al. (2023a).

145 At the Center for Environmental and Marine Studies (CESAM) of the University of Aveiro (Portugal), sugar species
146 were extracted from the filters with ultrapure Milli-Q water in ultrasonic agitation, as described by Oduber et al. (2021). After
147 the extraction, the solutions were filtered with syringe filters (PTFE; 0.2 μm) and transferred to vials for liquid chromatography



148 analysis with amperometric detection. Sugar compounds such as levoglucosan (Lev), mannosan (Man), galactosan (Gal),
 149 mannitol (Mnt), arabinol (Ara), and xylitol (Xyl) were determined with a Thermo Scientific Dionex™ ICS-5000 equipped with
 150 an anion-exchange analytical column (CarboPac® PA-1; 2 × 250 mm). Multi-step gradient conditions were adopted, with
 151 ultrapure Milli-Q water and two solutions of NaOH (200 mM and 5 mM). Recoveries were reported by Caseiro et al (2007).

152 2.3 Benzo(a)pyrene equivalent indexes

153 Benzo(a)pyrene equivalent indexes were calculated to evaluate toxicity parameters due to exposure to PAHs. Equations 1 and
 154 2 were employed to calculate the BaP_{TEQ} and BaP_{MEQ} by multiplying each species' concentrations by their toxic and mutagenic
 155 equivalency factors (TEF and MEF), as reported in de Oliveira Alves et al. (2020). The PAH carcinogenicity equivalent index
 156 (BaP_{Eq}) was also calculated by applying Equation 3, as adopted by Yassaa et al. (2001) and Cecinato (1997).

$$157 \text{BaP}_{\text{TEQ}} = ([\text{BaA}] \times 0.1) + ([\text{Chr}] \times 0.01) + ([\text{BbF}] \times 0.1) + ([\text{BkF}] \times 0.1) + ([\text{BaP}] \times 1) + ([\text{InP}] \times 0.1) + ([\text{DBA}] \times 5) + ([\text{BPe}] \times 0.01) \quad (1)$$

$$158 \text{BaP}_{\text{MEQ}} = ([\text{BaA}] \times 0.082) + ([\text{Chr}] \times 0.017) + ([\text{BbF}] \times 0.25) + ([\text{BkF}] \times 0.11) + ([\text{BaP}] \times 1) + ([\text{InP}] \times 0.31) + ([\text{DBA}] \times 0.29) + ([\text{BPe}] \times 0.19) \quad (2)$$

$$159 \text{BaP}_{\text{Eq}} = ([\text{BaA}] \times 0.06) + ([\text{BbF}] \times 0.07) + ([\text{BkF}] \times 0.07) + ([\text{BaP}] \times 1) + ([\text{DBA}] \times 0.6) + ([\text{InP}] \times 0.08) \quad (3)$$

160 2.4 Data treatment and Positive Matrix Factorization

161 Pearson coefficients were obtained to estimate the correlation between different variables (Jamovi software), and *r* was
 162 considered significant when *p* < 0.05. Correlations between 0.0 and 0.3 were considered negligible, between 0.3 and 0.5 as
 163 weak, between 0.5 and 0.7 as moderate, between 0.7 and 0.9 as strong, and between 0.9 and 1.0, as very strong (Khan et al.,
 164 2018). To evaluate equal and unequal variances, the Mann–Whitney U test was also employed (*p* < 0.05). Polar plots were
 165 constructed with the mass concentrations as functions of wind speed and direction (software R). Diagnostic ratios were
 166 performed between two (or more) chemical species concentrations: OC/EC, EC/Cu, PC/CTot, Fe/Ca²⁺, Cu/Sb, Cu/Zn, Fe/Cu,
 167 Sn/Sb, La/Ce, V/Ni, Pb/Cu, Cu/Ca²⁺, BaP/(BaP+BeP), Flt/(Flt+Pir), InP/(InP+BPe), BaA/(BaA+Cri), LMW-PAHs/HMW-
 168 PAHs, Pyr/BaP, Pyr/BbF, Flt/BbF, NO₃/EC, SO₄²⁻/NO₃⁻, SO₄²⁻/EC, K⁺/Lev, Lev/Man, SO₄²⁻/Zn, and NO₃⁻/Zn.

169 The ISORROPIA model calculates the composition and phase state of the water-soluble inorganic aerosol in
 170 thermodynamic equilibrium with gas phase precursors, simulating the process of dissolution of atmospheric particles and the
 171 ion formation (Bian et al., 2014; Fountoukis and Nenes, 2007; Li et al., 2014; Vieira-Filho et al., 2016a). In this study, the
 172 ISORROPIA II was applied. It can solve two types of problems: (i) forward (or "closed system") and (ii) reverse (or "open
 173 system"). The reverse problem approach was adopted in this study using aerosol phase concentrations of NH₃ (ammonium
 174 ion), H₂SO₄, Na⁺, Ca²⁺, K⁺, Mg²⁺, HCl, and HNO₃ to estimate water content, salt aerosol concentrations, and gaseous precursors
 175 aerosols. The aerosol-atmosphere system was considered thermodynamically stable (with precipitation of salts).

176 The enrichment factor (EF) is an approximation employed to identify the degree to which an element in the aerosol is
 177 enriched or depleted. It was calculated using aluminum as a soil tracer (Lee, 1999). Elements EF below 10 were considered to
 178 be of crustal origin (not enriched), and elements with EF above 10 were considered to be of non-crustal origin (anomalously
 179 enriched) (Pereira et al., 2007). Equation 4 is adopted to calculate EF, where C_{Xp} and (C_{Alp}) are the concentrations of elements
 180 X and Al in the sample, and (C_{Xc}) and (C_{Alc}) are their average concentrations in the Earth's crustal material:

$$181 \quad EF = \frac{\frac{C_{Xp}}{C_{Alp}}}{\frac{C_{Xc}}{C_{Alc}}} \quad (4)$$

182 The positive matrix factorization (PMF) receptor model was applied to the datasets (Paatero and Tapper, 1994),
 183 including ninety-four samples. The USEPA PMF5.0 software was used. The variable classification followed the established
 184 definitions: "bad" when the signal-to-noise ratio (S/N) was below 0.2, "weak" with S/N between 0.2 and 2, and "strong" when



185 S/N was above 2 (Lang et al., 2015). The number of samples below the detection limit (Amato et al., 2016; Contini et al., 2016;
186 Paatero and Hopke, 2003) and the thermal stability of the species (Pereira et al., 2017b) were also considered. Weak variables
187 had their uncertainty three-fold increased, and bad variables were excluded from the model (Norris et al., 2014). Twenty-two
188 species were considered as strong (NH_4^+ , K^+ , NO_3^- , SO_4^{2-} , V, Mn, Ni, Zn, As, Rb, Cd, Sb, Pb, Lev, OC1, OC2, OC3, OC4,
189 PC, EC1, EC2, and EC3), six species were classified as weak (Ca^{2+} , Mg^{2+} , Cu, EC4, LMW-PAHs, and HMW-PAHs) and the
190 concentrations of particulate matter were defined as a total variable (weak). Concentrations below the detection limits (DL)
191 were substituted by half of the DL value. Uncertainties were calculated following the procedure by Norris et al. (2014). To
192 evaluate the number of factors, Q robust (QR) was compared to Q theoretical value (QT) as in Pereira et al. (2017b). The final
193 model was obtained with an additional 7% modeling uncertainty. Solutions with three to eight factors were tested, and a final
194 solution with five factors was taken as the best result, with factors that could be well interpreted. Bootstrap mapping (BS) and
195 displacement of factor analysis (DISP) were used to analyze factor solutions, confirming a 5-factor solution as the most
196 feasible. Most of the markers used to identify the sources were within the BS interquartile ranges (box) and mapping ranged
197 from 87%-100%, furthermore, no DISP swaps were observed.

198 2.5 Backward air mass trajectories

199 For specific pollution events, backward air mass trajectories spanning 48 hours were generated using the HYSPLIT model
200 (Draxler and Rolph, 2003) via the READY (Real-time Environmental Applications and Display System) platform provided
201 by NOAA (National Oceanic and Atmospheric Administration). Trajectory frequencies were calculated to illustrate the origin
202 of air masses reaching the MASP in selected polluted periods, starting at 9:00 AM. The trajectories were calculated at a height
203 level of 500 and 3000 meters above ground level (AGL), based on GDAS meteorological fields with 1 degree resolution.

204 2.6 Ecotoxicity assays

205 The ecotoxicity of $\text{PM}_{2.5}$ was screened by the kinetic version of the *Aliivibrio fischeri* bioluminescence-based assay (Kováts et
206 al., 2021). This bioassay mimics the respiratory metabolism of biological systems resulting from exposure to particulate matter.
207 This assay provides an easy-to-quantify endpoint to assess the presence of toxic substances. Inhibition of the bacteria's
208 metabolism by toxic substances is demonstrated by the attenuation of its natural light emittance. Two 17 mm diameter filter
209 sections were cut and ground in an agate mortar. The samples were then transferred to 4 mL vials, to which 2 mL of ultra-pure
210 water was added. The suspensions were prepared with continuous agitation. The manufacturer's reconstitution solution was
211 used to rehydrate the lyophilized bacteria (strain NRRL-B-11177, from Lange Co.), which were then stabilized for 35 min at
212 12°C. For each sample, serial dilutions in 2% NaCl were prepared in 96-well plates. After adding the bacterial suspensions to
213 the samples, the bioluminescence intensity was continuously read for the first 30 seconds by a Luminoskan Ascent
214 Luminometer (Thermo Scientific). The bioluminescence was reread after 30 min of contact. The Ascent Software (Aboatox
215 Co., Finland) was employed to calculate the EC50 (concentration that causes 50% inhibition of bioluminescence compared to
216 the control). Depending on their toxic units ($\text{TU} = 100/\text{EC50\%}$), samples were cataloged as non-toxic ($\text{TU} < 1$), toxic ($1 < \text{TU}$
217 < 10), very toxic ($10 < \text{TU} < 100$), or extremely toxic ($\text{TU} > 100$).

218 3 Results and discussions

219 3.1 $\text{PM}_{2.5}$ chemical composition and general trend

220 The concentrations of particulate matter presented a wide variation. $\text{PM}_{2.5}$ concentrations ranged from 7 to 47 $\mu\text{g m}^{-3}$, averaging
221 24 $\mu\text{g m}^{-3}$ (Figure 2) and exceeding the new World Health Organization's (WHO) daily recommendations on 75% of sampling
222 days (15 $\mu\text{g m}^{-3}$), but none of national and local limits were surpassed (CONAMA, 2018; WHO, 2021). In terms of mass

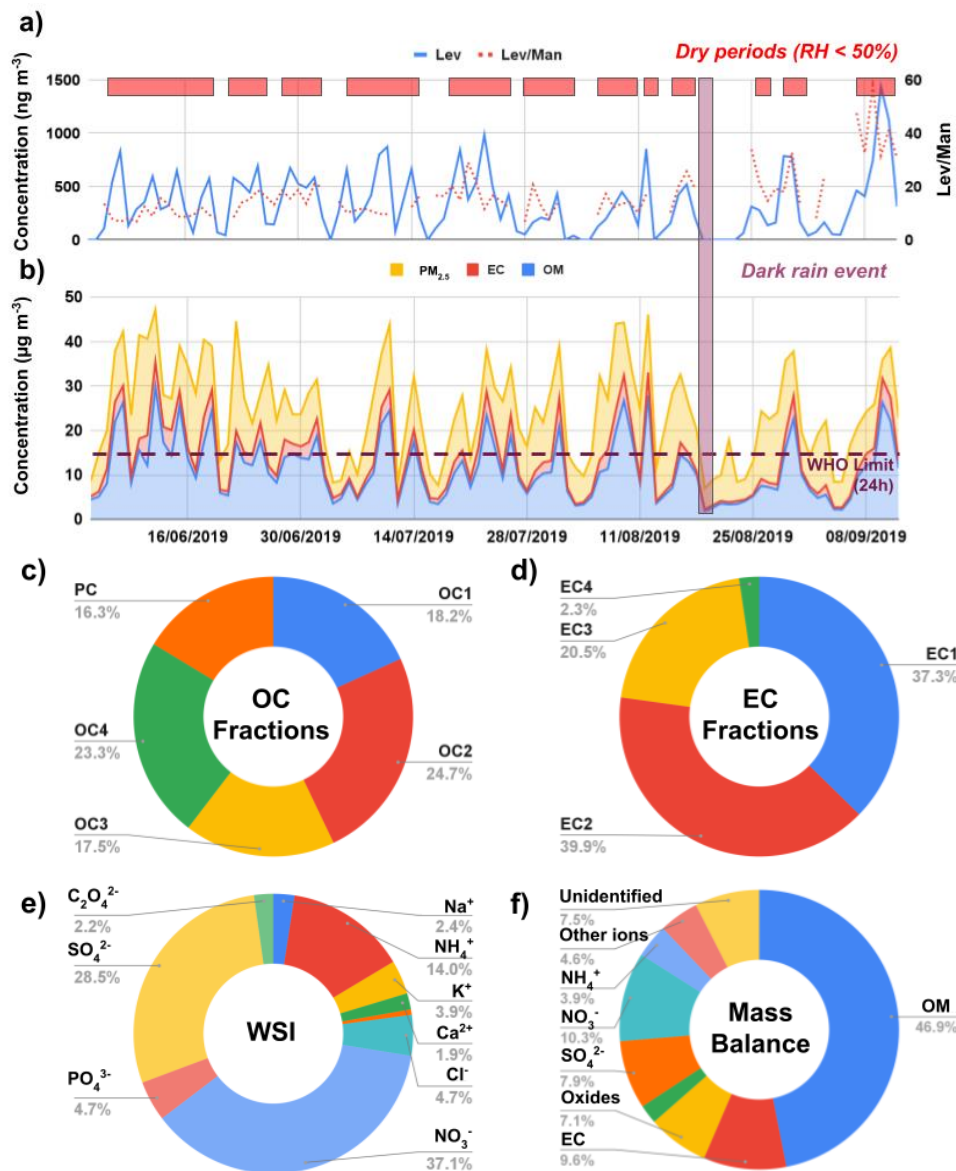


223 fractions, the most abundant elements observed in the 2019 intensive campaign were $K > Al > Cu > Fe$ (Table 1). The species
224 mentioned are linked to dust resuspension, vehicular sources, and biomass burning. Potassium (K) is connected to soil
225 resuspension and biomass burning, aluminum (Al) is related to soil resuspension, and iron (Fe) and copper (Cu) are associated
226 with vehicular sources in the MASP (Brito et al., 2013; Pereira et al., 2017b, 2023a, 2023b). As observed in the 2014 intensive
227 campaign, secondarily formed ions were the most abundant: $NO_3^- > SO_4^{2-} > NH_4^+$ (Figure 2e). However, the profile has
228 changed slightly, showing a greater abundance of nitrate over sulfate in most of the period, unlike the intensive campaigns of
229 2008, 2010, 2013, and 2014 (Table S2), when sulfate was predominant in PM (Pereira et al., 2019, 2017a,b, Souza et al., 2014).
230 The total mass of the most common element oxides was estimated (Al_2O_3 , SiO_2 , TiO_2 , MnO , and Fe_2O_3). Since Si was not
231 determined in this study, SiO_2 was estimated based on the Al content (three times the concentrations of Al_2O_3) (Alves et al.,
232 2018). The sum of these oxides can be used to estimate the proportion of crustal species in the $PM_{2.5}$ (Almeida et al., 2006)
233 and accounted for 7%.

234 A predominance of organic matter was observed in $PM_{2.5}$, accounting for a mass fraction of 47%, on average, followed
235 by NO_3^- and EC (nearly 10%) (Figure 2e). OM and EC represented a significant fraction of $PM_{2.5}$, over 50% on average.
236 Similarly, in the Eastern part of São Paulo (2019-2020), organic matter (OM) corresponded to nearly 40% of $PM_{2.5}$ (Vieira et
237 al., 2023). Previous studies (2008 and 2014) pointed to higher proportions of EC in $PM_{2.5}$ (Table S2). The elemental carbon
238 fraction is reducing worldwide (Chow et al., 2022a, Yamagami et al., 2019) (more details are presented in the SI) and a
239 reduction trend related to lower vehicular emissions of this species (Pereira et al., 2023a, 2023b). The emission limits following
240 a control program policy were upgraded in the early 2010s, similar to Euro 5 and Euro 4, for heavy-duty (HDVs) and light-
241 duty vehicles (LDVs), respectively (Pacheco et al., 2017) and more recently in 2022 (CETESB, 2022). The control policies
242 are associated with reducing carbonaceous species, especially EC (Pereira et al., 2023a,b). Furthermore, adopting biofuels
243 (e.g., ethanol and biodiesel blends) reduces these pollutants' emissions (de Abrantes et al., 2009). The relative reduction of
244 sulfate levels, together with EC, is observed worldwide, as reported in the SI. Following a similar trend to the observed in
245 other Latin American metropolises (Gómez-Peláez et al., 2020), the precursor SO_2 reduced relatively more than NO_x in the
246 MASP in the last decades (Andrade et al., 2017). The transport sector became the dominant SO_2 source in the MASP in the
247 last three decades after the reduction of industrial emissions following the adoption of electrical boilers (Kumar et al., 2016).
248 Since the early 2010s, S10 diesel, and S50 gasoline have been adopted to control vehicular emissions, although older trucks
249 were allowed to use S500 diesel (CETESB, 2015). From 2024, a resolution will establish new national specifications for road-
250 use diesel oils, discontinuing S500 fuels totally (MME, 2024).

251 The OC and EC fractions are shown in Figures 2c and 2d, respectively. A predominance of OC2 and OC4 was observed
252 among the organic carbon fractions and EC1 and EC2 among the elemental carbon fractions. The relatively low proportion of
253 EC3 suggests that this site is less affected by HDV emissions, since previous experiments in the MASP have shown that EC3
254 predominated in a diesel-powered HDV-impacted tunnel (Pereira et al., 2023b; Monteiro dos Santos et al., 2016). In the tunnel
255 studies, the OC2 fraction dominated the emissions and had already been observed in urban areas of São Paulo in 2013
256 (Monteiro dos Santos et al., 2016). OC1 is the most volatile fraction, which may explain its relatively lower proportion in the
257 particulate matter. Pyrolyzed carbon (PC) represented 16% of OC. Previously, PC represented 20-30% of total OC at the
258 university and downtown sites, accounting for less than 10% of OC in a street canyon (Monteiro dos Santos et al., 2016). This
259 fraction encompasses oxygenated components and links to water-soluble organic carbon (WSOC), secondary formation, and
260 primary sources, including biomass burning (Zhu et al., 2014; Pio et al., 2007; Yu et al., 2002). More recently, it has been
261 connected to HDV emissions, possibly due to the adoption of biodiesel (Pereira et al., 2023b).

262



263

264

265

266 **Figure 2:** Variation in the concentrations of Lev and Lev/Man ratio (a) and of $\text{PM}_{2.5}$, OM, EC (b), fractions of OC (c) and EC
 267 (d), ionic composition (e), and mass balance (f). In (a), "Dry periods" are marked with red squares (daily minimum RH <
 268 50%), and the dark rain event is marked in purple.

269

270

271



272 **Table 1:** Median, average, minimum, and maximum concentrations of different species and diagnostic ratios¹.

	Med.	Ave.	Min.	Max.		Med.	Ave.	Min.	Max.
($\mu\text{g m}^{-3}$)					(Cont.)				
PM_{2.5}	23.7	24.5	6.9	47.2	Cu	93	136	13	931
OC	6.3	7.2	1.2	18.6	Zn	39	49	4.0	250
EC	1.8	2.3	0.3	6.7	As	1.2	1.2	0.3	2.9
SOC	2.7	3.4	0	10.6	Se	1.1	1.4	0.1	5.7
(ng m^{-3})					Rb	1.8	2.2	0.1	6.2
Na⁺	143	166	5	549	Sr	4.6	5.2	0.3	15.4
NH₄⁺	737	954	61	4241	Mo	1.6	4.9	0.1	31.2
K⁺	247	268	6	686	Ag	0.27	0.26	0.01	0.85
Ca²⁺	101	128	17	517	Cd	0.49	0.66	0.03	2.69
Mg²⁺	44	43	6	95	Sn	5.5	8.2	0.2	30.7
Cl⁻	174	321	14	1505	Sb	3.8	5.7	0.3	27.9
NO₃⁻	2115	2531	134	10711	Ba	14	16	4	54
PO₄³⁻	320	318	36	784	La	0.25	0.29	0.01	1.47
SO₄²⁻	1651	1942	69	6139	Ce	0.23	0.26	0.01	2.09
C₂O₄²⁻	158	152	12	319	Tl	0.06	0.07	0.00	0.23
(ng m^{-3})					Pb	11	14	1	38
Lev	315	380	38	1437	Bi	0.16	0.2	0.01	0.9
Man	23	29	7	123	U	0.23	0.25	0.06	0.69
Gal	13	16	7	41	Ratios				
Xyl	6	8	2	75	OC/EC	-	3.1	1.1	10.2
(ng m^{-3})					EC/Cu	-	17.3	2.2	146.5
Al	180	208	11	1142	Fe/Ca²⁺	-	0.8	0.0	7.8
K	271	286	16	757	Cu/Sb	-	23.6	3.6	543.1
Ti	7.5	8.9	1.4	141	Cu/Zn	-	2.8	0.2	23.1
V	1.2	1.7	0.1	8.0	Fe/Cu	-	0.7	0.0	6.8
Cr	1.7	3.4	0.0	20.7	La/Ce	-	1.1	0.5	16.7
Mn	6	6.9	0.6	25	V/Ni	-	0.8	0.1	2.8
Fe	64	99	2	674	SO₄²⁻/NO₃⁻	-	0.8	0.0	4.9
Co	0.07	0.08	0.00	0.33	K⁺/Lev	-	0.7	0.0	4.7
Ni	1.5	2.0	0.2	27	Lev/Man	-	13	6.7	58

273

274

275

276

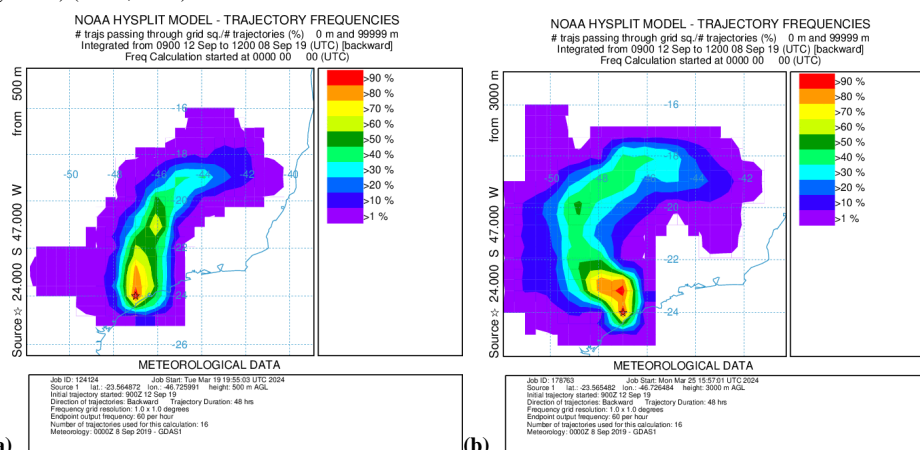
277

Levoglucosan, a monosaccharide anhydride widely used as a biomass-burning tracer, presented the highest average concentration (380 ng m^{-3}) among isomer sugars, followed by mannosan (29 ng m^{-3}). Compared to a previous intensive campaign (2014), the average K^+ level reduced from 809 ng m^{-3} to 268 ng m^{-3} (almost three-fold), while levoglucosan presented a similar level (509 ng m^{-3}). Since potassium levels are high in crop-burning emissions (Chow et al., 2022a), the significant

¹ Average diagnostic ratios were calculated with the average species' concentrations.



278 reduction in concentrations may be due to the lower influence of sugarcane burning since control policies have contributed to
 279 the decrease in the number of fires (Valente and Laurini, 2021). Galactosan was present in less than half of the samples,
 280 averaging 16 ng m^{-3} . It is usually observed in lower proportions than mannosan in biomass burning emissions (Bhattarai et al.,
 281 2019). The highest levoglucosan concentrations were observed on September 10 and 11 (1437 and 1119 ng m^{-3}) in a dry period
 282 that preceded a cold front. Relatively higher concentrations were also observed for K^+ on both days (543 and 555 ng m^{-3}). Back
 283 trajectories arriving at 500 m for these two days point to the typical influence of air masses from the north and northwest of
 284 São Paulo state (Figure 3), as observed in previous campaigns (Pereira et al., 2017a, 2017b). When a height above the boundary
 285 layer is considered (3000 m), it is possible to see a frequency of trajectories passing through areas in the country's central
 286 region. The states of Minas Gerais and Goiás, located north of São Paulo state, also presented many fires from September 10
 287 to 12 (Figure S2) (INPE, 2019).

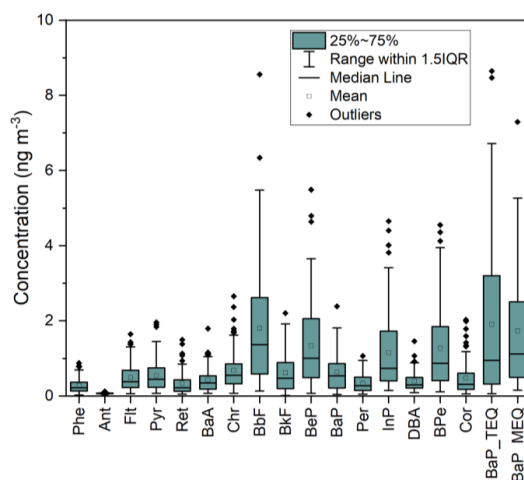


288

289 **Figure 3:** Backward trajectory frequencies for September 10 and 11, 2019, arriving at 500 m (a) and 3000 m (b).

290 Xylitol was the most detected polyol, with an average concentration of 8 ng m^{-3} . This species is mainly found in
 291 biological material, soil biota, and biomass-burning smoke (Caseiro et al., 2007). Other polyols were detected in a few samples,
 292 as discussed in SI. Arabitol and mannitol levels tend to increase in the wet season, contrary to what was observed for biomass-
 293 burning tracers in a medium-sized city in the São Paulo state (Carvalho et al., 2023). The study period is expected to have
 294 lower pollen-related emissions since these spore emissions are enhanced under higher temperatures and humidity (Marynowski
 295 and Simoneit, 2022).

296 The total concentration of PAHs in $\text{PM}_{2.5}$ ranged from 1.1 to 37.3 ng m^{-3} , with an average of 10.1 ng m^{-3} , higher than
 297 the one observed in the 2019 extensive campaign (including a wet period), of 4.7 ng m^{-3} (Serafeim et al., 2023). The most
 298 abundant compounds observed in the present study were BbF, BeP, and BPe (Figure 4 and Table S3), with BbF being
 299 potentially carcinogenic and related to emissions from gasoline-powered vehicles (Ravindra et al., 2008). The predominance
 300 of BbF is often observed in São Paulo. This compound is emitted in smaller amounts by LDVs than BaP (Pereira et al., 2023a).
 301 However, it is less influenced by chemical decomposition and more persistent (Aubin and Farant, 2000), and together with
 302 DBA, presents the most extended residence times in the atmosphere (Keyte et al., 2013).



303

304 **Figure 4:** Box plots of polycyclic aromatic hydrocarbon concentrations.

305 Benzo(a)pyrene averaged 0.6 ng m^{-3} (ranging from 0.04 to 2.39 ng m^{-3}) and surpassed the annual limit recommended
 306 by the European Environment Agency (1 ng m^{-3}) in 16% of the samples (Ravindra et al., 2008). However, half of the samples
 307 exceeded this value if the BaP toxicity equivalent index (BaP_{TEQ}) is considered (average of 1.9 ng m^{-3} and range of 0.06 - 8.64
 308 ng m^{-3}). The benzo(a)pyrene-equivalent index (BaP_{Eq}), calculated according to Yassaa et al. (2001), ranged between 0.04 and
 309 4.08 ng m^{-3} , with an average of 0.9 ng m^{-3} , lower than those determined for samples collected in winter in 2010, 2012, 2013
 310 and 2014 in São Paulo (ranging from 1.1 to 3.4 ng m^{-3}) (Pereira et al., 2017b, 2017a). This reduction may be attributed to
 311 emission regulations and adopting biofuels, such as ethanol and biodiesel, which can lower HMW-PAH emissions (de Abrantes
 312 et al., 2009; Pereira et al., 2023a). This trend follows a reduction in PAH emissions in recent decades in developed countries
 313 due to the establishment of new regulations (Shen et al., 2011). BaP_{MEQ} and BaP_{TEQ} tended to increase with northern and
 314 northwestern winds, more associated with drier weather, stable conditions, and biomass-burning-related aerosols (Figure S3).
 315 The opposite was observed with S and SE winds when cold fronts and sea breezes were registered.

316 3.3 Diagnostic ratios and polar plots

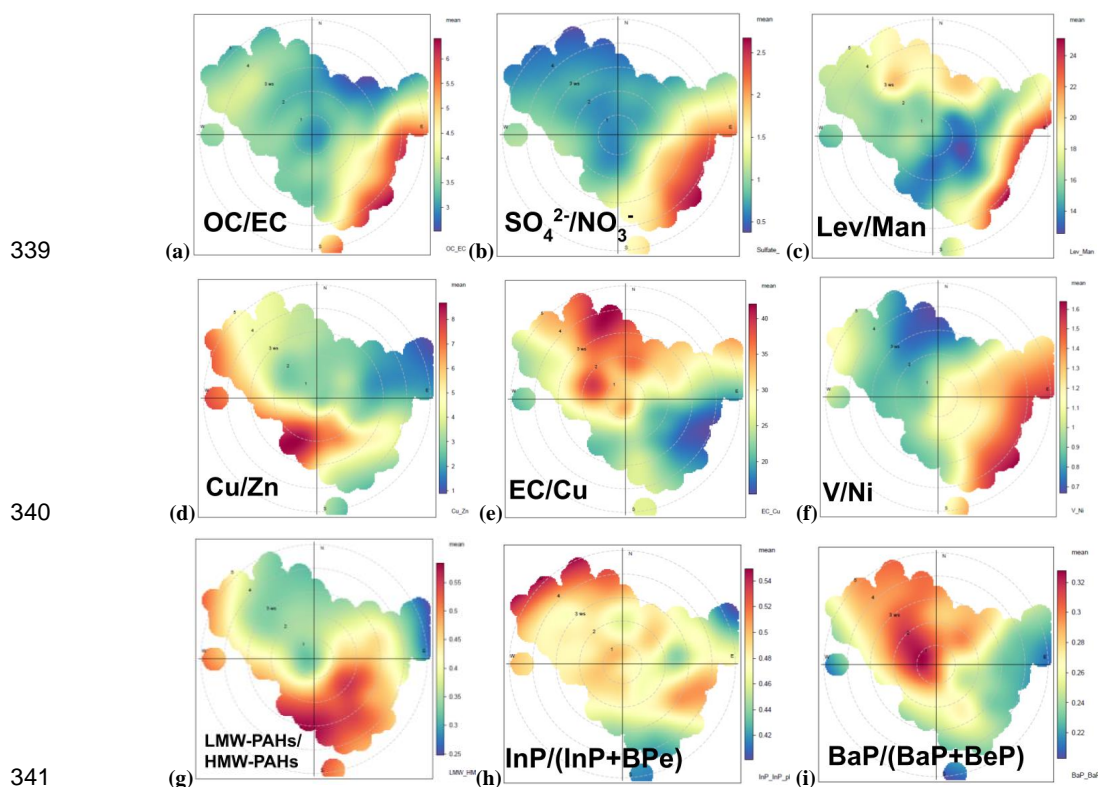
317 The OC/EC ratios in the present study ranged from 1.1 to 10.2, with an average of 3.1 (the monthly averages varied from 3.0
 318 to 3.3). In previous tunnel and roadside campaigns in the MASP, ratios lower than 1 were observed, increasing to nearly 2 in
 319 more background green areas, where there is increased biogenic influence and secondary formation (Brito et al., 2013;
 320 Monteiro dos Santos et al., 2016; Pereira et al., 2023b). The distance to main roads can increase the ratios and values between
 321 1.8 and 3.7 are found in background sites (Amato et al., 2016). However, biomass burning can also increase this ratio reaching
 322 over 4.1-14.5 (Watson et al., 2001; Wu et al., 2018). It is noteworthy that the values obtained in the present study were mostly
 323 higher than those found in the 2014, 2013, 2010, and 2008 intensive campaigns in the same sampling site (1.2-2.3)², in similar
 324 dry periods, however in shorter monitoring periods (Pereira et al., 2019, Pereira et al., 2017a,b; Souza et al., 2014). The ratio
 325 increase between these years may indicate a more significant influence of biofuel consumption and reduction of EC emissions
 326 (Pereira et al., 2023a), since the ethanol sales in the state of SP in 2019 were 75% higher than in 2013 (MME, 2023).
 327 Furthermore, an enhanced contribution from secondary organic carbon (SOC) formation may also contribute to this. SOC was
 328 estimated to reach nearly half of OC, with a maximum of 83% (Table 1). The formation of SOC is enhanced under higher

² Ratios (OC/EC and Lev/Man) were obtained for PM₁₀ in 2010 and 2013, with the assumption that most of these species are found in the fine fraction in São Paulo.



329 concentrations of oxidants such as ozone (Mbengue et al., 2023; Meng et al., 2021), which was observed in the MASP after
 330 2006 (Andrade et al., 2017). During the lockdown (2020), the OC/EC ratio increased (average of 5.7), following lower primary
 331 vehicular emissions and higher relative contribution of secondary processes (Farias et al., in review).

332 To investigate associations between wind direction and diagnostic ratios, polar plots were developed (Figure 5). The
 333 OC/EC ratios appeared to increase with relatively stronger SE winds (Fig 5a). These winds can also transport biogenic organic
 334 carbon from forested areas near the coast and air pollutants from coastal petrochemical and harbour areas. Furthermore,
 335 humidity can favor the partition of more polar SOC, as enhanced RH can lead to water uptake by hygroscopic submicron
 336 particles (Satsangi et al., 2021). In SE parts of MASP, more influenced by forests, less volatile oxidized organic aerosols were
 337 predominant and associated with SOC, derived from VOCs from both biogenic and vehicular sources (Monteiro dos Santos et
 338 al., 2021).



342 **Figure 5:** Polar plots considering the diagnostic ratios as a function of wind speed and direction for the ratios OC/EC (a),
 343 SO_4^{2-}/NO_3^- (b), Lev/Man (c), Cu/Zn (d), EC/Cu (e), V/Ni (e), LMW-PAHs/HMW-PAHs (g), InP/(InP+BPe) (h), and
 344 BaP/(BaP+BeP) (i). Distance from the center is related to wind speed and ratios increase from blue to red.

345 The average SO_4^{2-}/NO_3^- in this study was 0.8 (0.04–4.6), lower than the 1.6 (from July to December) of the 2019
 346 extensive study (Serafeim et al., 2023). The difference can be attributed to the lower temperatures in the present study (from
 347 June to September), which were less favorable to the volatilization of particulate nitrate (Tang et al., 2016). In 2014, higher
 348 ratios were observed, with 1.2 in the intensive period and 2.2 in the extensive period (Pereira et al., 2017b). The ratio in the
 349 2008 intensive campaign was higher than in 2014 (1.8) (Souza et al., 2014). Besides the ambient temperature, the reduction in
 350 this ratio can be associated with the relatively higher reduction of sulfur dioxide levels, if compared to nitrogen oxides (Sect.
 351 3.1). The ratio SO_4^{2-}/NO_3^- appeared to increase with SE and E winds (Figure 5b), suggesting that the production of sulfate was
 352 favored by humid and cloudier conditions associated with these air masses and/or a possible influence of sulfur dioxide



353 emitting sources in this area (e.g., industries and HDVs). Sulfate particles can grow with condensation by adding sulfate and
354 water in the aerosol droplet process (Guo et al., 2010). The SE part of MASP is influenced by industrial sources and high
355 sulfate levels associated with locally emitted SO₂ (Monteiro dos Santos et al., 2021).

356 Galactosan and mannosan are products of hemicellulose thermal decomposition, while levoglucosan is formed during
357 the combustion of cellulose (Simoneit, 2002). Since the amount of cellulose and hemicellulose varies with biomass type, with
358 hardwood containing relatively higher amounts of cellulose, the Lev/Man ratio can distinguish the smoke from different
359 biofuels (Li et al., 2021; Zhu et al., 2015). Typical ranges of 15–25 and 3–10 have been documented for hardwood and softwood
360 burning, respectively (Li et al., 2021). The average Lev/Man in the present study was 13 (6.7 - 58.0), slightly higher than
361 averages observed from 2014, 2013, and 2010 (ranging from 8 to 12)¹ (Pereira et al., 2017a,b, 2019). Previous ratios were
362 closer to the values found in chamber sugarcane burnings (10) and areas impacted by this type of smoke plumes (9) (Hall et
363 al., 2012; Urban et al., 2014). In an agroindustrial region in northern São Paulo state, a change in the Lev/Man ratio was
364 observed in 2020 (19) (Scaramboni, 2023), this increase was attributed to a change in the biomass burning profile, with reduced
365 sugarcane straw burning and increased use of sugarcane bagasse in power plants in the last decade (MME, 2024), alongside
366 the contribution of forest fires and other agricultural residue burnings. During high levoglucosan events at the end of the 2019
367 campaign, under lower relative humidity (Figure 1), the Lev/Man ratios exceeded 40 and suggested the influence of different
368 types of biomasses. Furthermore, in areas impacted by forest fires in the Amazon, likely related to hardwood, the ratios ranged
369 from 15 to 24 (Decesari et al., 2005; Graham, 2002). Before the dark precipitation event registered on August 19, associated
370 with smoke transported from areas in central Brazil and the Amazon (Pereira et al., 2021), Lev/Man values also reached values
371 above 20.

372 The median K⁺/Lev ratio was 0.7, considerably lower than that observed in the 2014 dry period (1.6) (Pereira et al.,
373 2017a). Lower K⁺/Lev ratios, typically below 1, have been found in emissions from wood stove combustion and forest fires
374 (Caseiro et al., 2009). Jung et al. (2014) reported similar K⁺/Lev ratios for hardwood and softwood burning (0.04 and 0.02,
375 respectively)², but this ratio was higher for crop burning (averaging 1.9)². Urban et al. (2012) documented an average ratio of
376 around 4 for fine sugarcane-burning particles³, justifying this value with the enrichment of K⁺ in the leaves and the inefficient
377 formation of levoglucosan during the flaming phase. The reduction in the proportion of K⁺/Lev in the present study may be
378 associated with reducing sugarcane burning after regulation. Some K⁺/Lev peaks were observed on days with very low Lev
379 concentrations (06/17, 07/27, 07/28, 08/06, and 09/01) (Figure S4), suggesting the influence of soil-related K⁺.

380 The Lev/Man ratio increased with stronger winds, whether from S/SE or N (Figure 5c), denoting the influence of
381 emissions from burning various types of biomasses. If the polar plot is obtained with Conditional Probability Function (CPF)
382 probability and Non-parametric Wind Regression (NWR), the increase with stronger N winds is prominent (Figure S5m and
383 S5n). The lowest ratios were found with low-speed SE winds, probably due to wood burning in some restaurants in that area.
384 Brazilian pizzerias traditionally use eucalypt logs in wood stoves. However, recently, briquettes have been adopted (Lima,
385 2015). Sun et al. (2019) reported Lev/Man ratios in the range of 17-19 for different types of briquettes. Some authors found
386 Lev/Man ratios mostly below 10 for woodstove emissions from different types of wood logs, while briquettes presented ratios
387 of 29.7 in hot start and 1.4 in cold start conditions (Gonçalves et al., 2011).

388 The diagnostic ratios EC/Cu, Fe/Cu, Cu/Zn, and Cu/Sb were associated with the proportion of LDVs and HDVs in
389 tunnels in the MASP (Pereira et al., 2023b). In previous studies, EC was more related to HDV emissions, while Cu was linked
390 to LDV emissions (Brito et al., 2013). EC/Cu ratios in the present varied between 2 and 146, and the average ratio was 17. It
391 was nearer the values observed for LDVs (5-8), rather than the ratios associated with a more HDV-impacted fleet (80-189).
392 Sb has been described as a tracer of abrasion sources, including brake wear (Thorpe and Harrison, 2008). Cu is also present in
393 Brazilian exhaust emissions from ethanol/gasohol vehicles (Brito et al., 2013). The present average Cu/Sb ratio was 24 (4-

³ These authors presented the ratios as Lev/K⁺.



394 543), higher than the median values observed in tunnels (11-14), which may be attributed to the distance of the sampling site
395 from a high-traffic area and a lower contribution from brake abrasion sources. The average Cu/Zn was 2.8 (0.2-23.1), falling
396 between the median value observed for LDV (6.2) and that documented for HDV+LDV-impacted tunnels (0.9). The Cu/Zn
397 and Cu/Sb ratios increased with southern weak winds (Figures 5d and S5f), suggesting an enrichment in copper and
398 predominance of LDV emissions in this area, possibly associated with the traffic of vehicles in the nearby residential
399 neighborhood. On the other hand, the EC/Cu and Fe/Cu ratios increased with N winds (Figures 5e and S5g), which may
400 indicate an influence of HDVs passing in the expressway located north of the campus.

401 The average V/Ni ratio was 0.8 (0.1-2.8). Higher values are found for residual fuel oil combustion range from 1 to 3
402 (Johnson et al., 2014). This ratio increased with strong E/NE/SE winds (Figure 5f), suggesting an influence from oil burning
403 in industries located in these areas (Vieira et al., 2023; Souto-Oliveira et al., 2021). The La/Ce ratio, similarly to the latter, was
404 favored by S/SE winds (Figure S5h). Higher ratios (4.3) were observed for fluidized-bed catalytic cracking (FCC) during
405 petroleum refining, while a lower value (0.7) was documented for automobile catalyst emissions (Kulkarni et al., 2006). A
406 petrochemical complex in the southeastern area of the MASP may explain this influence (Caumo et al., 2022; Gioia et al.,
407 2017). Previous studies have observed that cold fronts may be associated with isotopic fingerprints from the Cubatão
408 petrochemical industrial area outside the MASP (Souto-Oliveira et al., 2018).

409 Diagnostic ratios between PAHs for the analyzed samples were calculated and shown in Table S3. BaP/(BaP+BeP)
410 values lower than 0.5 indicate that the analyzed particles were aged, as BaP undergoes photolysis more quickly than BeP
411 (Tobiszewski and Namieśnik, 2012). The median was equal to 0.32, suggesting a predominance of aged particles. In three
412 samples (collected on 27/07, 03/08, and 28/08), this ratio was close to 0.5, indicating fresh emissions. The Flt/(Flt+Pir) median
413 was 0.48. According to De La Torre-Roche et al. (2009), values of this ratio ranging from 0.4 to 0.5 are characteristic of the
414 burning of fossil fuels. InP/(InP+BPe) median ratio was equal to 0.48, similar to what was observed in 2014 by Pereira et al.
415 (2017b). Values between 0.2 and 0.5 are associated with emissions from the burning of fossil fuels (Yunker et al., 2002). The
416 BaA/(BaA+Cri) presented an average of 0.38, falling near the observed for vehicular sources (0.2-0.35) (Akyüz and Cabuk,
417 2010).

418 Σ LMW-PAHs/ Σ HMW-PAHs median ratio was 0.35, within the range reported for pyrogenic (<1) emissions by some
419 authors (Zhang et al., 2008). However, this ratio was previously found to vary with the proportions of LDVs and HDVs (0.7
420 and 7.5, respectively) (Pereira et al., 2023b) and with ambient temperature (Tobiszewski and Namieśnik, 2012). The ratios
421 Pyr/BaP, Pyr/BbF, and Flt/BbF were associated with the proportion of LDVs and HDVs, increasing with the latter (Pereira et
422 al., 2023b). Nevertheless, the ratios can be influenced by the volatilization of Pyr and Flt in warmer conditions and the
423 photodegradation of BaP. The values were similar to those observed for gasoline emissions (near or below 1).

424 Σ LMW-PAHs/ Σ HMW-PAHs and Pyr/BaP ratios appeared to be affected by winds coming from NW (Figures 5g and
425 S5i), with a mixed biomass burning and vehicular influence, and by cooler winds from the S, which may favor the condensation
426 of LMW-PAHs in the particulate phase (Ravindra et al., 2008). Temperature was the meteorological parameter that most
427 affects total and individual PAHs, with a more substantial influence on LMW-PAHs (Amarillo and Carreras, 2016).
428 InP/(InP+BPe) ratios approached the values (above 0.5) found for grass, wood, and coal combustion with NW winds (Yunker
429 et al., 2002). It was not possible to observe the same for Flt/(Flt+Pyr), which increased with S and SE winds, suggesting that it
430 may be linked with the cooler/cloudier conditions and the shorter photochemical residence time of Pyr compared to Flt (Keyte
431 et al., 2013). The highest BaP/(BaP+BeP) values were registered for lower wind speeds, suggesting fresh local emissions
432 (Tobiszewski and Namieśnik, 2012), although it also increased with stronger NW winds.

433 3.4 Source apportionment (PMF)

434 The factor profiles obtained by Positive Matrix Factorization are shown in Figure 6. A 5 factor solution was obtained, with
435 two factors associated with vehicular emissions (VE1 and VE2), one associated with biomass burning (BB), secondary



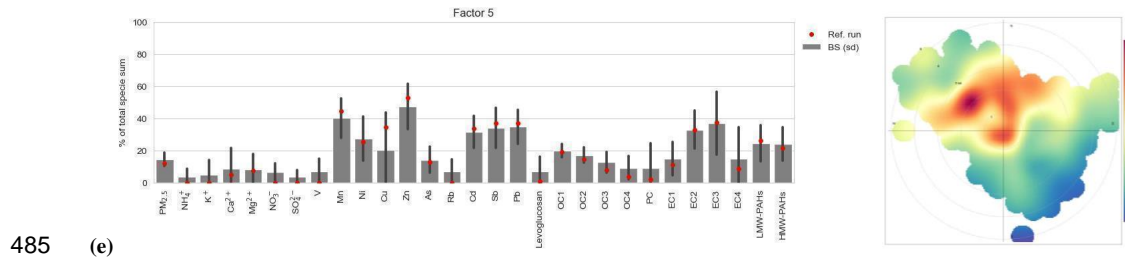
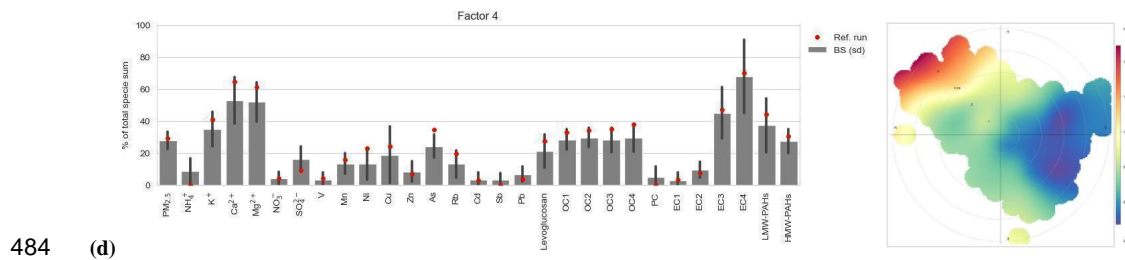
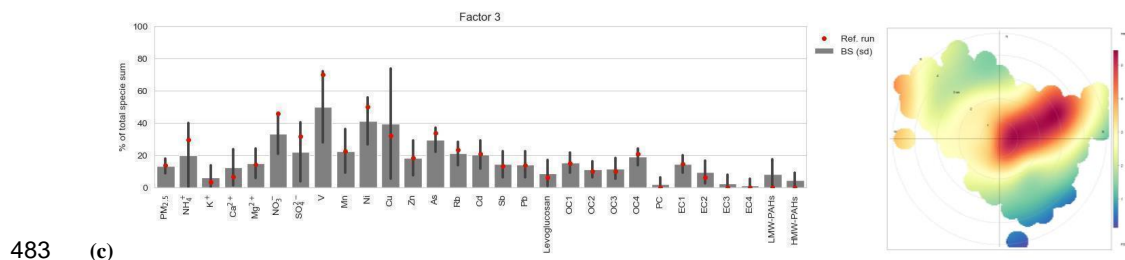
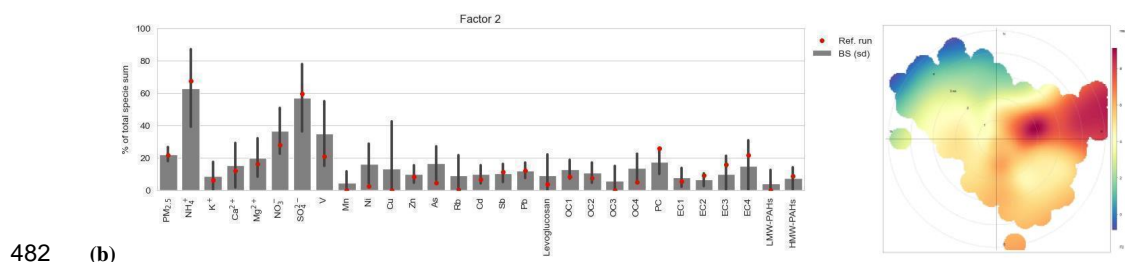
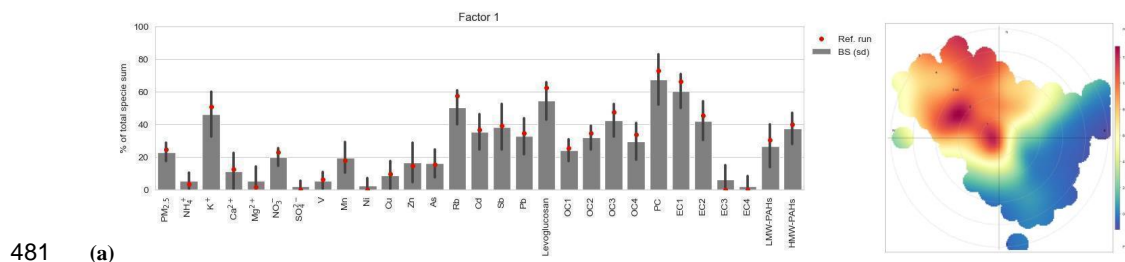
436 formation (SF) and industries. Factor 1 (BB) was characterized by biomass-burning-related species such as levoglucosan, K^+ ,
437 and some carbonaceous species (Bhattarai et al., 2019; Simoneit, 2002). However, the presence of Cd, Sb, and Pb suggests a
438 mixture with vehicular sources (Thorpe and Harrison, 2008) or that these species may be linked with waste burning (La Colla
439 et al., 2021). This factor was also characterized by a significant contribution from pyrolyzed carbon, a fraction of water-soluble
440 organic carbon (WSOC), often associated with biomass burning and SOA (Yu et al., 2002; Zhu et al., 2014). Among elemental
441 carbon fractions, EC1 was the most abundant. Some elements, such as Rb, also appeared in the biomass burning profile. This
442 species has been described as a component of some types of soil by Calvo et al. (2013), wood-burning emissions (Fine et al.,
443 2001), and biomass burning aerosols in the Amazon (Artaxo et al., 1994). Recently, water-soluble rubidium in fine particulate
444 matter has been assigned to wood-burning emissions and considered an alternative biomass-burning tracer (Massimi et al.,
445 2020). This factor increased with winds coming from N and NW, corroborating the influence of the transport of biomass-
446 burning aerosols from the countryside and forested areas in northern and central Brazil. It decreases with S and SW winds,
447 suggesting a reduction with cold fronts and sea breezes (Sánchez-Ccoyllo et al., 2002). The results agree with Souto-Oliveira
448 et al., (2023), that showed the impact of the transport of wildfires to the MASP during fine particulate matter exceedance
449 events in 2020.

450 Factor 2 (SF) was highly loaded with secondary formation species, mainly NH_4^+ and SO_4^{2-} . Furthermore, this factor
451 also presented loadings of some primary emission species, such as vanadium. Serafeim et al. (2023) also observed high
452 loadings for Ni and V in the secondary-related factor in the MASP. These species originate mainly from industrial emissions
453 (Calvo et al., 2013). Previously, it has been observed with the WRF-Chem model that secondary formation explains 20 to 30%
454 of $PM_{2.5}$ in the MASP (Vara-Vela et al., 2016), increasing in the summertime (Pereira et al., 2017b). Factor 3 showed high
455 loads for V, Ni, and nitrate. Earlier studies in the MASP have associated Ni and V with residual oil burning and industrial
456 sources (Andrade et al., 1994; Castanho and Artaxo, 2001). Heavy oil combustion in industrial boilers also emits nickel and
457 zinc, especially in the ultrafine fraction (smaller than $0.1 \mu m$) (Jang et al., 2007; Linak et al., 2004). Factor 3 (IN) increased
458 with the same wind direction as Factor 2 (SF), which suggests that it may be partially related to secondary formation, possibly
459 due to emissions of precursor gases, such as NO_x and SO_2 , or associated with the same air masses. Secondary aerosol formation
460 can mislead the separation of factors in PMF, as observed by Faisal et al. (2024).

461 Factor 4 (VE1) was loaded with soil resuspension constituents, such as Ca^{2+} and Mg^{2+} , as well as with species previously
462 related to vehicular emission in MASP, such as As and Cu, carbonaceous species (OC1, OC2, OC3, OC4, EC3, and EC4),
463 LMW-PAHs and HMW-PAHs (Pereira et al., 2017b, 2023a, 2023b). In the extensive 2019 campaign, an independent road
464 dust factor was observed, representing 32% of $PM_{2.5}$ (Serafeim et al., 2023). The association with construction-related calcium,
465 found in concrete material, can also be considered (Bourotte et al., 2006). EC3 and EC4 were abundant in this factor. EC3 was
466 anteriorly related to HDV emissions in MASP, while EC4 was found in an urban canyon. Furthermore, OC2, OC3, and OC4
467 were found in LDV emissions in similar proportions (Monteiro dos Santos et al., 2016; Pereira et al., 2023a). Levoglucosan
468 was also observed in a smaller proportion in this factor. As observed in 2014, this factor overlaps with factor 1 (Pereira et al.,
469 2017b), as they increase with the same wind direction. However, the contribution of factor 4 increases with NW stronger
470 winds, corroborating the resuspension of road dust as the main source. Strong NW winds are often attributed to prefrontal
471 conditions (Ribeiro et al., 2018). Another aspect contributing to the overlap is that this anhydrosugar is also found in the PM_{10}
472 from the wear between tires and pavements, given that wheel rubbers have cellulose in their composition (Alves et al., 2020).
473 However, $PM_{2.5}$ -bound levoglucosan is emitted in much smaller proportions by this non-exhaust vehicle emission source
474 compared to biomass burning (Bhattarai et al., 2019). The “hybrid” factor may occur because the aerosol in the urban
475 atmosphere, comprising mainly vehicular-related species, road dust, and biomass burning emissions, arrives mixed at this
476 semi-background site. Additionally, it is challenging to differentiate HDV from LDV emissions in this site (Pereira et al.,
477 2017a). Enhancing the time resolution may facilitate this separation through techniques (e.g., Aerosol Mass Spectrometer)
478 (Monteiro dos Santos et al., 2021). Proportionally, non-exhaust emissions, such as road dust, will increase in the future (Thorpe



479 and Harrison, 2008) since exhaust emissions are on a downward trend due to increasingly stricter regulations and improved
 480 treatment systems.



486 **Figure 6:** Profiles identified with the PMF receptor model and polar plots (a-e).



487

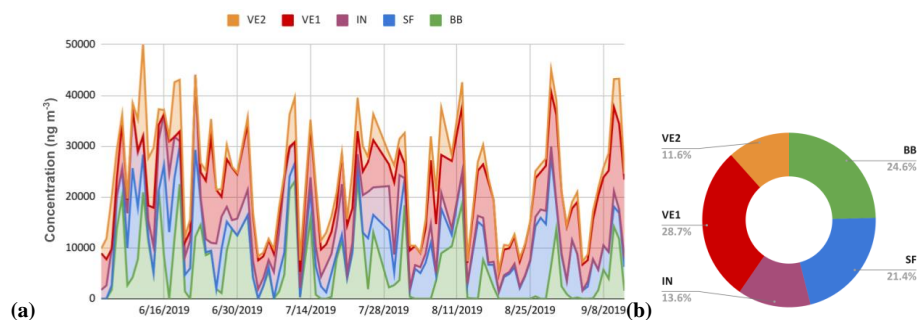
488

Factor 5 (VE2) presented several species of vehicular origin, such as Mn, Ni, Cu, Zn, Sb, and the potentially toxic Cd and Pb (Brito et al., 2013; Pereira et al., 2023a), in addition to OC and EC fractions, especially EC3, the latter being more associated with HDVs (Pereira et al., 2023b). This vehicular factor increased with lower wind speed, suggesting a local contribution. The site is located next to an avenue with a constant flow of buses and LDVs during the day and is near a busy expressway. Despite the lower proportion, the emissions of buses and trucks contributed to almost half of black carbon in the MASP (Brito et al., 2018). In the SEM study performed by Bourotte et al. (2006), particles rich in carbon, Cu, and Zn were identified and associated with incomplete fossil fuel burning. Zinc is also enriched in tire wear particles, as zinc oxide is added to the tires in the vulcanization process (Thorpe and Harrison, 2008). Copper was previously assigned to LDV exhaust emissions and to the corrosion of the internal parts of the MASP fleet engines (Ferreira da Silva et al., 2010). It was also pointed out as a brake dust particle tracer (Thorpe and Harrison, 2008).

498

Figure 7 shows the contributions of each type of source to PM_{2.5} and their variation between sampling days. Biomass burning accounted for 25% of PM_{2.5}. This contribution was slightly higher than that documented in the intensive campaign of 2014 (18.3%). In the extensive study performed in 2019 (including dry and wet seasons), the biomass burning factor represented 13% of ambient PM_{2.5}, a similar share to that observed in the 2014 extensive period (Pereira et al., 2017b; Serafeim et al., 2023), and lower than the one of the intensive campaign between June and September of the present study, a period typically more affected by biomass burning (Pereira et al., 2017a). Several peaks of the biomass burning factor coincided with lower RH values. An increase in the contribution of this factor was observed two days before the sky-darkening phenomenon at MASP on August 19, when dark precipitation was recorded, attributed to pollutants emitted by biomass burning (Pereira et al., 2021).

506



507

Figure 7: Daily factor contribution (a) and PM_{2.5} contributions (b) identified with the PMF receptor model.

508

The vehicular-related sources, such as local LDVs and HDVs (12%), vehicular emissions plus road dust (29%), and secondary formation (21%), represent a significant share of particulate matter in the city (over 60%), similar to that observed in 2013, 2014 and 2015 (Souto-Oliveira et al., 2021; Emygdio et al., 2018; Pereira et al., 2017a). The factor VE1 increased throughout the sampling period and dominated PM_{2.5} at the end of August and the beginning of September, indicating greater dust resuspension at the end of winter as a result of the long dry spell and higher wind speeds (Figure S6). In another source apportionment study performed in the east region of São Paulo in 2019, four factors were found to contribute to PM_{2.5}, with a similar high contribution of vehicular sources (Vieira et al., 2023) and an increase of soil particles in the dry season: heavy-duty vehicles (42%), light-duty vehicles (9.9%), soil and local particles (38.7%) and local sources (8.6%). According to Serafeim et al. (2023), vehicular emissions and biomass burning were associated with enhanced oxidative potential. Contrastingly, secondary aerosol was predominant in São Paulo during the 2020 lockdown (nearly 40%), followed by biomass burning (30%), with a relative reduction of the contribution of vehicular sources (Farias et al., in review).

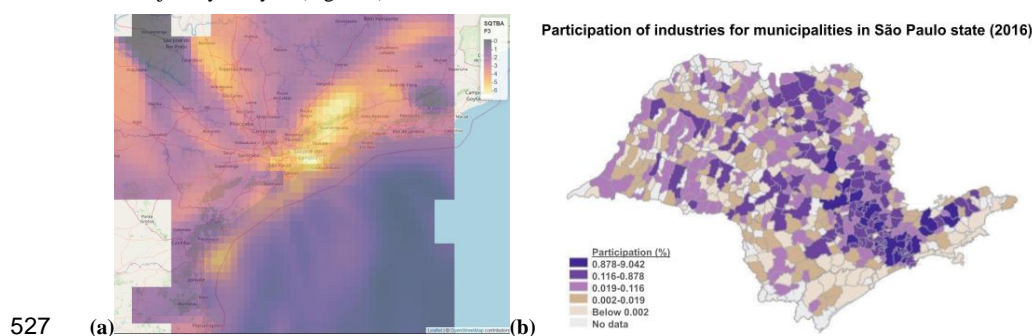
520

Industrial sources accounted for only 13.6%, a similar level to that observed in 2014 (over 10%). A relatively low impact of industrial emissions is felt in this part of the city, as nowadays, industries are located on the outskirts of the MASP

521



522 and the countryside (Kumar et al., 2016) and no large industries are found near the sampling site. Thus, the contribution of this
 523 factor, combined with the frequencies of the trajectories, suggested the influence from areas to the east and northeast, including
 524 parts of MASP and other neighboring metropolitan areas with a high concentration of industries. The Simplified Quantitative
 525 Transport Bias Analysis (SQTBA) approach was adopted, it recognises the plume dispersion process, considering it as part of
 526 back trajectory analysis (Figure 8).

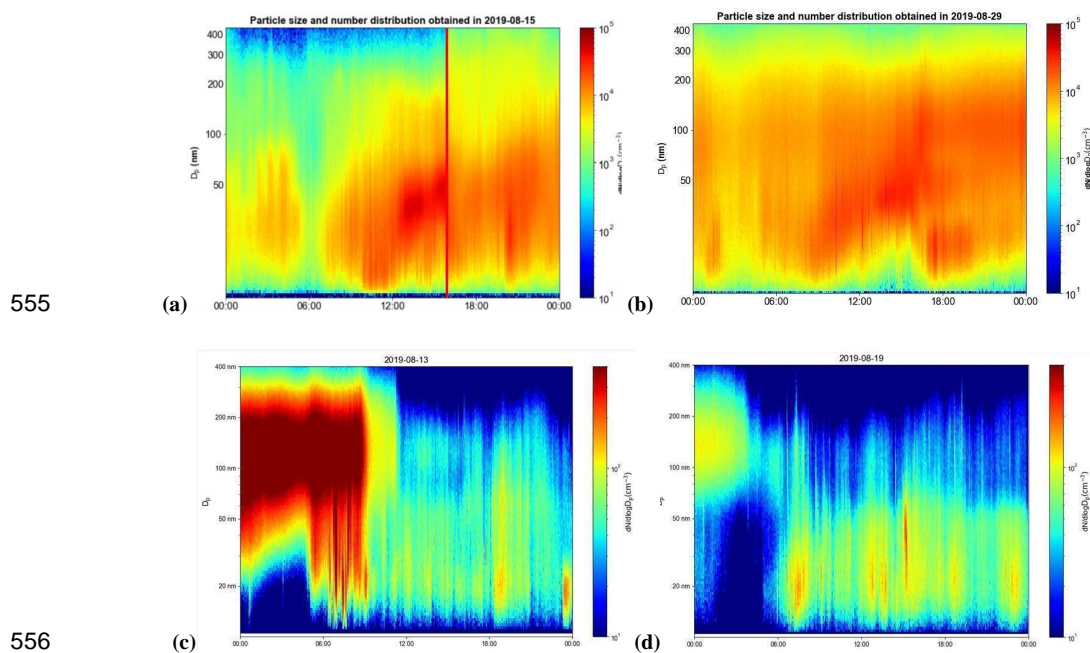


527 (a) (b)
 528 **Figure 8:** Trajectory analysis for the contribution of factor 3 (a), and participation of industries for municipalities in São Paulo
 529 state (industrial transformation value), adapted from SEADE (2019) (b).

530 3.5 Pollution events and particle size distribution

531 Submicrometer particle number size distributions were monitored between June 27 and September 12, 2019. The Aitken mode
 532 (diameter range between 50 and 100 nm, approximately) contributed to the largest share of total particles number
 533 concentration, averaging 46%, ranging from 21 to 73 %. The nucleation mode (diameter below 30 nm) contributed the least to
 534 the total, with 21%, ranging from 0 to 49%. The accumulation mode (diameter above 100 nm, approximately) accounted, on
 535 average, for 32%, ranging from 12 to 68% (Table S4). Nearly 70% of the monitored particles presented a diameter below 100
 536 nm, classified as ultrafine particles, which can penetrate the extensive area of the lungs and can reach other organs through the
 537 lung vasculature (Schraufnagel, 2020). The predominance of Aitken mode particles suggests the influence of relatively fresh
 538 particles, in comparison to the typically aged accumulation mode particles. A previous study in the MASP reported associations
 539 between inorganic species and Aitken mode particles, whereas aged oxygenated organic particles were mostly associated with
 540 the accumulation mode (Monteiro dos Santos et al., 2021), the accumulation mode increased during high particulate matter
 541 conditions, while the nucleation mode presented a smaller increase and was related to local traffic. The conditions promoting
 542 high PM concentrations (low boundary layer height, weak ventilation, absence of precipitation, and clear conditions) lead to
 543 secondary aerosol production and increase of particles due to condensation (Sánchez-Ccoyllo and Andrade, 2002; Santos et
 544 al., 2018). Thus, the dominance of larger geometric mean diameters in the present study (between Aitken and accumulation
 545 modes) may be associated with the condensation in the surface of pre-existing particles, which can also suppress nucleation
 546 (Monteiro dos Santos et al., 2021).

547 On August 15 and 29, dominated by secondary inorganic formation as observed in the PMF analysis (Figure 7), new
 548 particle formation events were observed based on the contour analysis of the size and number distributions of aerosols obtained
 549 with the SMPS (Figure 9a and 9b). Additionally, the sea breeze entry around 4 PM local time (marked by the vertical red line
 550 in Figure 9a) was observed, which reduced the particle number concentration from 1.8×10^4 to $1.0 \times 10^4 \text{ cm}^{-3}$ and increased
 551 the geometric mean diameter from 44.2 ± 2.0 to 47.0 ± 2.2 nm within approximately one hour. Secondary inorganic species
 552 are typically partitioned between Aitken and accumulation modes. In the study performed in 2016/2017, a large fraction of
 553 particles was in the Aitken mode, likely from the reaction of nitric acid and ammonia emitted by vehicles (Carbone et al., 2013;
 554 Monteiro dos Santos et al., 2021).



555 **(a)** 00:00 06:00 12:00 18:00 00:00 **(b)** 00:00 06:00 12:00 18:00 00:00
 556 **(c)** 00:00 06:00 12:00 18:00 00:00 **(d)** 00:00 06:00 12:00 18:00 00:00
 557 **Figure 9:** Submicrometer particle number size distributions for August 15 **(a)**, 29 **(b)**, 13 **(c)**, and 19 **(d)**. The x-axis represents
 558 the timeline (local time), the y-axis refers to particle diameters and the colors represent the number of particles, normalized by
 559 diameter bins.

560 On August 13 and 19, the arrival of cold fronts altered the particle size profile and reduced $PM_{2.5}$ levels (Figures 9c,
 561 9d, S7a, and S7b). On August 13, the total particle number concentration dropped from 2.8×10^4 at 7 AM to 0.5×10^4 at 11
 562 AM, according to SMPS data. The distribution, which had a geometric mean diameter of 94.7 ± 2.0 nm at 8 AM, shifted to
 563 particles with a mean size of 43.8 ± 2.2 nm. On August 19, there was an event of darkened rain after the transport of biomass-
 564 burning smoke from central and northern regions of Brazil and collision with more humid air masses coming from the ocean
 565 due to a cold front causing the formation of low-level clouds (Pereira et al., 2021). Before this event, an increase of BB and
 566 VE1 factors contributions was observed.

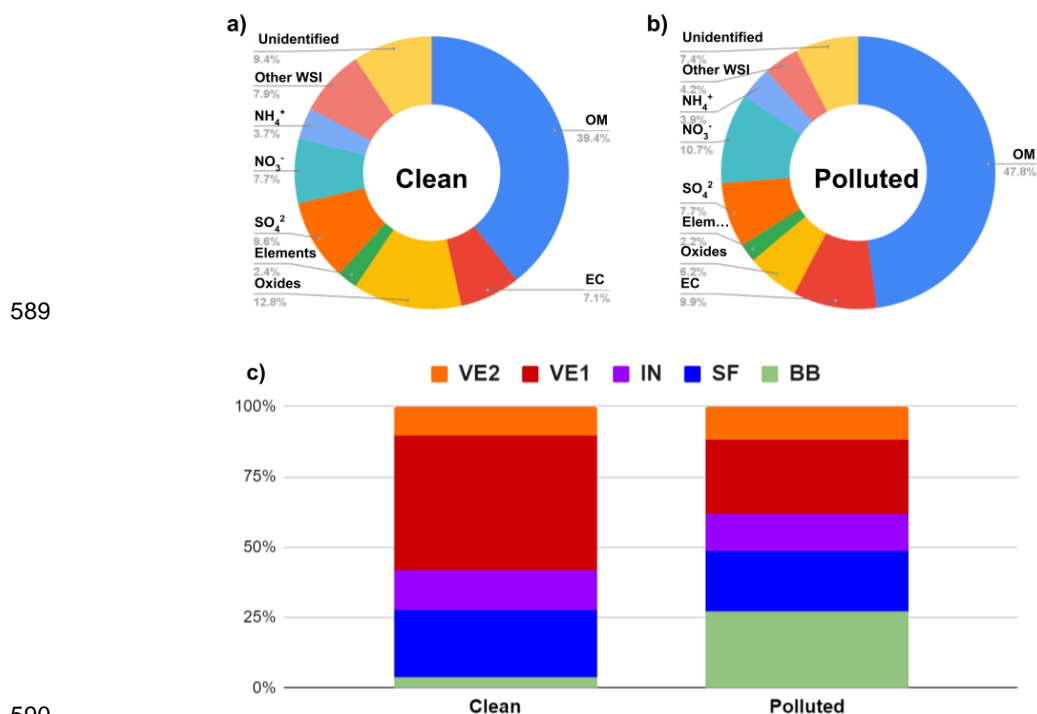
567 3.6 Chemical and source characteristics of pollution event days

568 The sampling days were separated between high pollution days (with $PM_{2.5}$ above the WHO guideline of $15 \mu g m^{-3}$) and low
 569 pollution days (below). These polluted periods were associated with relatively higher average temperature and lower humidity
 570 ($19^\circ C$ and 74%, compared to $15^\circ C$ and 83%) During these pollution events, $PM_{2.5}$ increased by 171%, and carbonaceous
 571 species (OM+EC) represented a higher mass fraction (nearly 60%) (Figure 10). In polluted periods, the accumulation processes
 572 can lead to the formation of organic coatings on black carbon particles (Monteiro dos Santos et al., 2021). On the other hand,
 573 oxides, other WSI, and sulfate accounted for a higher fraction in non-event days. The unidentified fraction, which can be
 574 attributed to unmeasured components such as carbonate or water (Pereira et al., 2017a), was also slightly higher in non-event
 575 days. In absolute numbers, all PMF factors increased on event days. However, the BB factor contribution increased
 576 significantly on polluted days, rising from 4 to 27% of the $PM_{2.5}$ mass.

577 OC, EC, K^+ , NO_3^- , V, Mn, Fe, Co, Zn, Rb, Cd, Sn, Sb, Ce, Tl, Pb, and Lev presented a significantly higher increase
 578 than that observed for $PM_{2.5}$ in these polluted periods (Figure S8), suggesting an accumulation of these species during these
 579 events ($p < 0.05$). In percentage terms, all OC and EC fractions increased more than $PM_{2.5}$ ($p < 0.05$), except OC1, EC3, and



580 EC4. Proportionally, retene increased less than $PM_{2.5}$, suggesting that it may be linked to a local biomass-burning source, such
 581 as wood burning in restaurants (Andrade et al., 2017; Kumar et al., 2016). Mannosan followed the same trend. The toxicity
 582 indexes BaP-TEQ and BaP-MEQ presented significant increases ($p < 0.05$), caused mainly by the rise in HMW-PAHs due to
 583 the accumulation of fossil-fuel and biomass burning emitted aerosols (Vasconcellos et al., 2010). Furthermore, there appears
 584 to have been an accumulation of other toxic species, such as potentially toxic elements (PTE) such as Cd, Sb, and Pb, from
 585 anthropogenic sources (Pereira et al., 2023b; Thorpe and Harrison, 2008). However, the toxicity unity (TU) did not increase
 586 as much (~50%). Fosfate was the only species to decrease, although with $p > 0.05$. It is often associated with dust and farming
 587 activities (Yuan et al., 2008; Allen et al., 2010). In the present study, the most likely origin was in the soil.
 588



590
 591 **Figure 10:** Chemical mass balance for clean ($PM_{2.5} < 15 \mu g m^{-3}$) (a) and polluted days ($PM_{2.5} \geq 15 \mu g m^{-3}$) (b), and PMF source
 592 contributions for both periods (c).

593 Levoglucosan concentration tripled during the polluted days (423 and 140 ng m^{-3} , respectively). Ionic potassium
 594 quadrupled these days (330 and 82 ng m^{-3}), suggesting a higher impact of crop burning (Chow et al., 2022a). However,
 595 levoglucosan represented similar portions of OM on both occasions (nearly 3%). Xylitol and mannosan presented a lower
 596 increase on polluted days ($p < 0.05$), suggesting that they are associated with other types of biomass burning (Sect. 3.3). In
 597 2020, it was observed that during smoke plume events in the MASP, $PM_{2.5}$ surpassed $25 \mu g m^{-3}$ at 99% of the air quality
 598 monitoring stations. These days, the plumes are mainly associated with sugarcane burning and often with the contribution of
 599 wildfires in the Amazon and Pantanal biomes (Souto-Oliveira et al., 2023). In that study, the authors were able to differentiate
 600 CO_2 from local wood burning (4-7%) from that from remote forest wildfires (4-26%). In recent years, the influence of remote
 601 forest burning has occurred, likely related to natural seasonal variations and climate change, with lower humidity and
 602 precipitation and increased fires (Goss et al., 2020, Abram et al., 2021). The influence of biomass burning in the metropolitan



603 area often occurs above the boundary layer. However, these plumes from remote regions can still influence the concentration
604 and composition of PM_{2.5} at the surface (Souto-Oliveira et al., 2023).

605 Overall, there was an increase in the enrichment factors of metals in the polluted period, five times higher for Fe and
606 similar for U (Figure S9), suggesting that these are mostly soil-bound in the clean period. Se, Sb, and Bi presented the highest
607 enrichment factors in all periods, reaching values near and above 10,000. Selenium was previously attributed to industrial
608 sources in the eastern part of the MASP (Vieira et al., 2023). It was also assigned to human activities (fossil fuel, burning of
609 garbage, tires and paper, coal combustion, oil, and glass industries) (Mehdi et al., 2013). Ti, Fe, and Co presented the lowest
610 EFs (near and below 1). La and Ce displayed relatively low enrichment factors (below 5). K and V, Ni, and Rb got close to
611 the EF of 10 in the polluted period.

612 3.7 Correlations between PMF results and other variables

613 The factors obtained with the PMF receptor model were correlated with other variables: meteorological data (temperature,
614 relative humidity, and wind) collected from the local station, concentrations of chemical species, diagnostic ratios and results
615 obtained from the ISORROPIA thermodynamic model (modeled solid and liquid inorganic aerosol, water content, NaNO_{3(s)},
616 Na₂SO_{4(s)}, NaHSO_{4(s)}, NaCl_(s), NH₄Cl_(s), NH₄NO_{3(s)}, (NH₄)₂SO_{4(s)}, NH₄HSO_{4(s)}, CaSO_{4(s)}, Ca(NO₃)_{2(s)}, CaCl_{2(s)}, K₂SO_{4(s)},
617 KHSO_{4(s)}, KNO_{3(s)}, KCl_(s), MgSO_{4(s)}, Mg(NO₃)_{2(s)}, MgCl_{2(s)}, H⁺_(aq), Na⁺_(aq), NH₄⁺_(aq), Cl⁻_(aq), NO₃⁻_(aq), SO₄²⁻_(aq), HSO₄⁻_(aq), Ca²⁺_(aq),
618 K⁺_(aq) and Mg²⁺_(aq) (Table S5 and Figure S10). Overall, the components were negatively correlated with RH and positively with
619 temperature, which typically indicates dry air masses and unfavorable conditions for the dispersion of atmospheric pollutants
620 (Sánchez-Ccoyllo et al., 2002), more discussions are presented in the SI.

621 The biomass burning factor correlated with BPe and InP, species typically associated with vehicular emissions
622 (Ravindra et al., 2008). However, the InP/(BPe+InP) polar plots suggested an influence of biomass burning with northwest
623 strong winds (Sect. 3.3). The low correlation of retene with BB and levoglucosan suggests that this species may be related to
624 a local biomass-burning source or the influence of gas-particle partition of this semi-volatile species (Ravindra et al., 2008).
625 Chloride was moderately correlated with BB and VE2 factors ($r > 0.5$), strongly correlated with mannosan and EC1 ($r > 0.7$),
626 and weakly correlated with levoglucosan, suggesting a different biomass burning profile, such as wood burning in restaurants
627 or biomass burning associated with waste (Kumar et al., 2015). Xylitol was weakly correlated with BB and VE1 ($r > 0.3$).
628 Notably, it presented weaker correlations with potassium than Lev, suggesting a biomass-burning origin less associated with
629 crop burning.

630 The secondary aerosol formation factor was moderately correlated with the modeled liquid inorganic aerosol and water
631 content of the aerosol, in addition to the modeled secondary species NH₄⁺_(aq), SO₄²⁻_(aq), and HSO₄⁻_(aq) ($r > 0.6$). Correlation with
632 modeled water content suggests that the secondary formation pathway in São Paulo depends on humidity. SO₄²⁻ and NO₃⁻
633 formation in clouds and fog droplets is mainly due to the heterogeneous aqueous transformation of SO₂ and NO_x under high
634 relative humidity (RH) during haze episodes (Huang et al., 2016). Among the ratios, the secondary formation factor presented
635 weak to moderate correlations with NO₃⁻/EC, SO₄²⁻/EC, and NO₃⁻/Zn ($r > 0.4$), suggesting that they can be helpful in identifying
636 secondary formation events, an opposite trend to that observed for the BB, VE1, and VE2 factors.

637 The IN factor presented moderate correlations with the liquid inorganic aerosol and water content in the aerosol,
638 possibly associated with more humid air masses coming from the east, as particles can grow in the aerosol droplet process
639 (Guo et al., 2010). Notably, it was correlated with aerosol acidity (H⁺_(aq)), perhaps due to gaseous oxides that can undergo
640 secondary reactions and produce acidic species. H⁺_(aq) was also moderately correlated with nitrate, suggesting an influence of
641 nitric acid (Ianniello et al., 2010). Selenium was moderately associated with the IN factor. This species was previously
642 attributed to industrial sources (Vieira et al., 2023). Sn was moderately correlated with IN ($r \sim 0.5$) and strongly correlated with
643 Tl. The IN factor presented a weak correlation with the V/Ni ratio ($r \sim 0.5$), denoting the contribution from the burning of crude
644 oil (Johnson et al., 2014). IN was also moderately correlated with NO₃⁻/EC, suggesting a connection with secondary formation.



645 There was a weak correlation between SF and IN, pointing to a common origin between both, maybe due to the emission of
646 gaseous precursors and secondary formation.

647 The PMF factor associated with vehicular exhaust and dust resuspension (VE1) presented weak correlations with most
648 species. The factor presented moderate correlations with the modeled mass of solid inorganic aerosol ($r \sim 0.6$). This factor
649 also displayed a moderate positive correlation with temperature ($r > 0.6$) and negative with relative humidity and pressure ($r <$
650 -0.5), suggesting an increase of this factor during prefrontal conditions. Among the factors, VE2 and BB presented higher
651 correlations with the toxicity equivalent indexes BaP-TEQ and BaP-MEQ ($r > 0.5$), suggesting a contribution of these sources
652 to carcinogenicity and mutagenicity. The correlations of VE2 were higher for BaA and HMW-PAHs such as Per, InP, BPe,
653 and Cor ($r > 0.5$), which are found in LDV emissions (Pereira et al., 2023a). La was moderately associated with VE2, and
654 strongly with Mn, Co, and Ce. La and Ce derive mainly from catalyst emissions (Kulkarni et al., 2006). Fe presented strong
655 correlations with VE2, and Ti, Mn, and Ce. These species are linked to vehicular and soil-related sources (Pereira et al., 2017a,
656 Brito et al., 2013). Co, a component of tire debris (Thorpe and Harrison, 2008), was moderately correlated with VE2 and
657 strongly correlated with La, Tl, and Mn. VE2 presented moderate correlations with Fe/Ca^{2+} ($r \sim 0.6$), which may indicate
658 enrichment of anthropogenic iron (Pereira et al., 2023a).

659 Some species were less source-specific. PO_4^{3-} presented no correlations with PMF factors and was moderately
660 correlated with Na^+ and Ca^{2+} ($r > 0.45$). Oxalate was not correlated with specific factors. It presented moderate correlations
661 with NH_4^+ , K^+ , NO_3^- , SO_4^{2-} , As, Rb, Sb, Tl, Pb, and OC ($r > 0.5$), suggesting multiple sources, as previously observed, such as
662 vehicle exhaust, biomass burning, and biogenic activity, in addition to secondary formation (Guo et al., 2010). Na^+ , as
663 previously observed in the MASP (Vieira-Filho et al., 2016b), was not specific for any source and presented a weak correlation
664 with some other species (Ca^{2+} , Cl⁻, PO_4^{3-} , As, Rb, Sr, and Cd) ($r > 0.3$), without strong correlation with Cl⁻, which can be
665 explained by the relatively low influence of sea spray in this site. Aluminium displayed low correlations with the PMF factors
666 and was strongly correlated with Ti ($r > 0.7$) and moderately with Ce ($r > 0.6$), pointing to an origin in crustal materials (Hetem
667 and Andrade, 2016). Ti was also strongly correlated with Ce. Both species presented low enrichment, suggesting a mineral
668 origin (Figure S8), apart from vehicular emissions. Cr was not source-related but presented a relatively high correlation with
669 Ni ($r \sim 0.5$). Both species were previously associated with industrial sources (Bourotte et al., 2011; Castanho and Artaxo, 2001).
670 Arsenic, a highly toxic element, showed relatively moderate correlations with BB, IN, and VE2 and strong with Rb, Ag, and
671 Cd. Arsenic has multiple sources, including industries (Calvo et al., 2013).

672 3.8 Ecotoxicity assays

673 Ecotoxicity tests of aqueous particulate matter extracts were performed with the bacteria *Aliivibrio fischeri*. All samples in this
674 study were classified as toxic, with toxic unity (TU) values ranging from 1.7 to 7.1, averaging 3.7. The highest values were
675 obtained in periods impacted by biomass burning (Figure S11). The TU unit showed moderate correlations with levoglucosan,
676 water-soluble K^+ , and the modeled aqueous K^+ ($r > 0.5$), which may be associated with biomass burning aerosols and water-
677 soluble organic species (not quantified in the study) (Urban et al., 2012). Among the factors obtained by receptor modeling,
678 biomass burning had the highest correlation with TU (Table S5), indicating that water-soluble components trigger the toxicity
679 of particles emitted by this source. The vehicular-exhaust factor exhibited the second highest correlation with TU, although
680 weak. In addition, the TU values presented moderate correlations with elements known to be toxic and associated with
681 vehicular sources such as Pb ($r \sim 0.5$). The correlation was moderate ($r > 0.5$) with OC (higher for fractions OC2, OC3, and
682 OC4, less volatile and more oxidized) and EC (higher for fractions EC1 and EC2). Significant correlations between the
683 bioluminescence inhibition responses and the contributions of biomass burning and traffic to particulate matter concentrations
684 were also reported for Coimbra, Portugal (Alves et al., 2021). As observed in the present study, toxicity was statistically
685 correlated with OC, EC, anhydrosugars, and elements from exhaust and non-exhaust emissions. Since biomass burning and
686 traffic emissions may elicit acute toxic effects, adopting source-specific preventive and remedial measures is necessary.



687 **4 Summary and conclusions**

688 Fine particulate matter (PM_{2.5}) was collected in a 100-day dry period in 2019, covering the period from June to early September,
689 when several pollution events were observed, surpassing the WHO daily limit of 15 µg m⁻³ in 75% of the days. Chemical
690 characterization was obtained, including water-soluble ions, elements, carbonaceous species, anhydrosugars, and polycyclic
691 aromatic hydrocarbons. Additionally, the size distribution of particles (SMPS) was monitored simultaneously. PM_{2.5} levels
692 were, however, lower than in previous studies. The lower sulfate-to-nitrate ratios suggested a decrease in sulfur oxide levels.
693 A higher contribution of organic matter to particulate matter indicated an increase in the secondary formation of organic species
694 and a reduction of elemental carbon emissions by vehicles. However, a further study should be performed to statistically assess
695 this trend over the last decades.

696 As for biomass burning, typically observed in the dry period there was a decrease in the contribution of sugarcane
697 straw burning, since there was a change in the K⁺/Lev and Lev/Man ratios and relatively lower potassium levels. However, the
698 long-range transport of plumes from forest fires and agricultural burning in regions north and northwest of MASP remains a
699 significant source of PM_{2.5} in this period, as the average concentration of levoglucosan remained high. Other authors have
700 observed a further increase in the influence of bagasse-burning plants and the intrusion of aerosols from forest fires originating
701 in central and northern Brazil. This last phenomenon is related to climate change and has increased in the last decades (longer
702 dry periods). The increase in the Lev/Man ratio with stronger winds suggests the contribution of different types of biomasses.
703 Correlations with other species and the PMF receptor model suggested Rb as a reliable biomass-burning tracer. PAHs remain
704 a concern due to increasing concentrations and equivalent toxicity values exceeding 1 ng m⁻³ in half of the samples. However,
705 the levels are lower than those observed in previous studies. The vehicular-related species BbF remained an abundant PAH,
706 suggesting it is a persistent constituent. PAH diagnostic ratios fell within the range observed for vehicular emissions. The
707 increased concentrations of these pollutants are likely related to the lower dispersion in this season. Additionally, increasing
708 V/Ni and La/Ce ratios with east and southeast winds suggested a contribution of aerosols from petrochemical industrial areas,
709 which can occur with meteorological conditions characterized by cold fronts and sea breezes.

710 The PMF receptor model was applied to assess the PM_{2.5} sources and a five-factor solution was obtained (biomass
711 burning, secondary formation, industrial, vehicular+road dust, and local vehicular). A high contribution of biomass burning,
712 associated with north and northwest winds, was observed, reaching one-fourth of the particulate matter. Considering the
713 previous source apportionment studies, sources related to vehicular emissions are still dominant (more than 60% of PM_{2.5}). A
714 mixed factor of road dust and vehicular emissions increased throughout the campaign, suggesting a more significant influence
715 of resuspension at the end of the winter. Relatively lower, an industrial contribution was observed, increasing with northeast
716 winds that pass through industrial areas of MASP. The PMF solution showed overlapping contributions in some factors, which
717 may be related to the low temporal resolution of sampling and the fact that emissions from various sources mix before reaching
718 the semi-background receptor site. Enhancing the time resolution in future investigations may help the identification of more
719 sources (e.g., Aerosol Mass Spectrometer).

720 Two particle formation events were identified by SMPS in days with pronounced secondary formation and happened
721 before the arrival of the sea breeze. The sulfate secondary formation was related to humid conditions, as suggested by
722 correlations between the contribution of secondary formation and the aerosol's modeled water content (ISORROPIA). During
723 days of pollution events (PM_{2.5} > 15 µg m⁻³), carbonaceous species represented a higher fraction of particulate matter, while
724 sulfate's contribution was reduced. An accumulation of PAHs and toxic species such as Cd, Sb, and Pb on these days represents
725 a health concern. These pollution events were associated with a relative increase in the contribution of the biomass burning
726 factor, whose emissions, added to pollutants emitted and formed locally, contribute to the degradation of air quality in the dry
727 season. Throughout the sampling campaign, all samples were classified as ecotoxic. The ecotoxicity correlated with the
728 biomass burning factor, highlighting the importance of regulating this source for air quality control. These results indicate that



729 controlling PM_{2.5} exceedance events should include regulating emerging biomass burning sources and stricter rules concerning
730 vehicular emissions.

731

732 **Data availability**

733 The datasets will be available upon request after publishing.

734

735 **Author contributions**

736 GMP performed part of the analyses (OC, EC, elements, and water-soluble ions), the data treatment and led the manuscript
737 writing. MFA managed the project, provided infrastructure, designed the study and revised the manuscript. PCV provided
738 infrastructure, designed the study and revised the manuscript. LYK performed the data treatment. RFB monitored the particle
739 size distribution and contributed with the writing. DMS helped with the OC and EC determination and revised the manuscript.
740 TSS performed the PAHs extraction and characterization. CG characterized the anhydrosugars. ICR performed the ecotoxicity
741 essays and helped with the revisions. CA, NK, LR, PA, and EDF provided infrastructure and revised the manuscript. TN,
742 RMM, and MAY revised the paper.

743

744 **Competing interests**

745 The authors declare that they have no conflict of interest.

746

747 **Acknowledgements**

748 These results were part of the “Chemical and toxicological SOURCE PROfiling” of particulate matter in urban air project
749 (SOPRO, Grant no. POCI-01-0145-FEDER-029574), supported by the Portuguese Foundation for Science and Technology
750 from the Ministry of Science, Technology, and Higher Education (FCT/MCTES), and by the São Paulo Research Foundation
751 (FAPESP; Grant #2018/07848-9). SOPRO project was also funded by FEDER, through COMPETE2020—Programa
752 Operacional Competitividade e Internacionalização (POCI), and by national funds (OE), through FCT/MCTES. The authors
753 also acknowledge FAPESP for Grants #2016/18438-0 (Metroclima project, for research resources) and #2019/01316-8
754 (URBESP project, scholarship), and National Research Council for the grants (CNPq 301503/2018-4). The financial support
755 to CESAM by FCT/MCTES (UIDP/50017/2020 + UIDB/50017/2020 + LA/P/0094/2020), through national funds, is also
756 acknowledged. Meteorological data (irradiance, atmospheric pressure, temperature and relative humidity) were kindly
757 provided by the IAG-USP meteorological station and the Climatology and Biogeography Laboratory (Department of
758 Geography - FFLCH - USP).

759 **References**

760 Abram, N.J., Henley, B.J., Sen Gupta, A., Lippmann, T.J.R., Clarke, H., Dowdy, A.J., Sharples, J.J., Nolan, R.H., Zhang, T.,
761 Wooster, M.J., Wurtzel, J.B., Meissner, K.J., Pitman, A.J., Ukkola, A.M., Murphy, B.P., Tapper, N.J., Boer, M.M.:
762 Connections of climate change and variability to large and extreme forest fires in southeast Australia, *Commun. Earth Environ.*,
763 2, 1-17, <https://doi.org/10.1038/s43247-020-00065-8>, 2021.

764 de Abranches, R., Vicente de Assunção, J., Pesquero, C. R., Bruns, R. E. and Nóbrega, R. P.: Emission of polycyclic aromatic
765 hydrocarbons from gasohol and ethanol vehicles, *Atmos. Environ.*, 43(3), 648–654,
766 <https://doi.org/10.1016/j.atmosenv.2008.10.014>, 2009.

767 Akyüz, M. and Cabuk, H.: Gas-particle partitioning and seasonal variation of polycyclic aromatic hydrocarbons in the
768 atmosphere of Zonguldak, Turkey., *Sci. Total Environ.*, 408(22), 5550–5558, <https://doi.org/10.1016/j.scitotenv.2010.07.063>,
769 2010.

770 Allen, A.G., Cardoso, A.A., Wiatr, A.G., Machado, C.M.D., Paterlini, W.C., and Baker, J.: Influence of intensive agriculture
771 on dry deposition of aerosol nutrients, *J. Braz. Chem. Soc.*, 21, 1, <https://doi.org/10.1590/S0103-50532010000100014>, 2010.



- 772 Almeida, S. M., Pio, C. A., Freitas, M. C., Reis, M. A. and Trancoso, M. A.: Approaching PM_{2.5} and PM_{2.5-10} source
773 apportionment by mass balance analysis, principal component analysis and particle size distribution., *Sci. Total Environ.*,
774 368(2–3), 663–674, <https://doi.org/10.1016/j.scitotenv.2006.03.031>, 2006.
- 775 Alves, C., Rienda, I. C., Vicente, A., Vicente, E., Gonçalves, C., Candeias, C., Rocha, F., Lucarelli, F., Pazzi, G., Kováts, N.,
776 Hubai, K., Pio, C. and Tchepel, O.: Morphological properties, chemical composition, cancer risks and toxicological potential
777 of airborne particles from traffic and urban background sites, *Atmos. Res.*, 264, 105837,
778 <https://doi.org/10.1016/j.atmosres.2021.105837>, 2021.
- 779 Alves, C. A., Evtyugina, M., Vicente, A. M. P., Vicente, E. D., Nunes, T. V., Silva, P. M. A., Duarte, M. A. C., Pio, C. A.,
780 Amato, F. and Querol, X.: Chemical profiling of PM₁₀ from urban road dust., *Sci. Total Environ.*, 634, 41–51,
781 <https://doi.org/10.1016/j.scitotenv.2018.03.338>, 2018.
- 782 Alves, C. A., Vicente, A. M. P., Calvo, A. I., Baumgardner, D., Amato, F., Querol, X., Pio, C. and Gustafsson, M.: Physical
783 and chemical properties of non-exhaust particles generated from wear between pavements and tyres, *Atmos. Environ.*, 224,
784 117252, <https://doi.org/10.1016/j.atmosenv.2019.117252>, 2020.
- 785 Amarillo, A. C. and Carreras, H.: Quantifying the influence of meteorological variables on particle-bound PAHs in urban
786 environments, *Atmos. Pollut. Res.*, 7(4), 597–602, <https://doi.org/10.1016/j.apr.2016.02.006>, 2016.
- 787 Amato, F., Alastuey, A., Karanasiou, A., Lucarelli, F., Nava, S., Calzolari, G., Severi, M., Becagli, S., Gianelle, V. L., Colombi,
788 C., Alves, C., Custódio, D., Nunes, T., Cerqueira, M., Pio, C., Eleftheriadis, K., Diapouli, E., Reche, C., Minguillón, M. C.,
789 Manousakas, M.-I. and Querol, X.: AIRUSE-LIFE+: a harmonized PM speciation and source apportionment in five southern
790 European cities, *Atmospheric Chemistry and Physics*, 16(5), 3289–3309, <https://doi.org/10.5194/acp-16-3289-2016>, 2016.
- 791 Andrade, F., Orsini, C. and Maenhaut, W.: Relation between aerosol sources and meteorological parameters for inhalable
792 atmospheric particles in Sao Paulo City, Brazil, *Atmos. Environ.*, 28(14), 2307–2315, [https://doi.org/10.1016/1352-2310\(94\)90484-7](https://doi.org/10.1016/1352-2310(94)90484-7), 1994.
- 794 Andrade, M.F., Kumar, P., de Freitas, E. D., Ynoue, R. Y., Martins, J., Martins, L. D., Nogueira, T., Perez-Martinez, P., de
795 Miranda, R. M., Albuquerque, T., Gonçalves, F. L. T., Oyama, B. and Zhang, Y.: Air quality in the megacity of São Paulo:
796 Evolution over the last 30 years and future perspectives, *Atmos. Environ.*, 159, 66–82,
797 <https://doi.org/10.1016/j.atmosenv.2017.03.051>, 2017.
- 798 Andrade, M.F., de Miranda, R.M., Fornaro, A., Kerr, A., Oyama, B., de Andre, P.A., Saldiva, P. Vehicle emissions and PM_{2.5}
799 mass concentrations in six Brazilian cities. *Air Qual. Atmos. Health*, 5, 79-88, <https://doi.org/10.1007/s11869-010-0104-5>,
800 2012.
- 801 Artaxo, P., Gerab, F., Yamasoe, M. A. and Martins, J. V.: Fine mode aerosol composition at three long-term atmospheric
802 monitoring sites in the Amazon Basin, *J. Geophys. Res.*, 99(D11), 22857, <https://doi.org/10.1029/94JD01023>, 1994.
- 803 Aubin, S. and Farant, J. P.: Benzo[b]fluoranthene, a potential alternative to benzo[a]pyrene as an indicator of exposure to
804 airborne PAHs in the vicinity of Söderberg aluminum smelters., *J. Air Waste Manag. Assoc.*, 50(12), 2093–2101,
805 <https://doi.org/10.1080/10473289.2000.10464236>, 2000.
- 806 Bhattarai, H., Saikawa, E., Wan, X., Zhu, H., Ram, K., Gao, S., Kang, S., Zhang, Q., Zhang, Y., Wu, G., Wang, X., Kawamura,
807 K., Fu, P. and Cong, Z.: Levoglucosan as a tracer of biomass burning: Recent progress and perspectives, *Atmos. Res.*, 220,
808 20–33, <https://doi.org/10.1016/j.atmosres.2019.01.004>, 2019.
- 809 Bian, Y. X., Zhao, C. S., Ma, N., Chen, J. and Xu, W. Y.: A study of aerosol liquid water content based on hygroscopicity
810 measurements at high relative humidity in the North China Plain, *Atmospheric Chemistry and Physics*, 14(12), 6417–6426,
811 <https://doi.org/10.5194/acp-14-6417-2014>, 2014.
- 812 Bourotte, C., Forti, M. C., Melfi, A. J. and Lucas, Y.: Morphology and solutes content of atmospheric particles in an urban
813 and a natural area of São Paulo state, Brazil, *Water Air Soil Pollut.*, 170(1–4), 301–316, <https://doi.org/10.1007/s11270-005-9001-1>, 2006.
- 815 Bourotte, C. L. M., Sánchez-Ccoyllo, O. R., Forti, M. C. and Melfi, A. J.: Chemical composition of atmospheric particulate
816 matter soluble fraction and meteorological variables in São Paulo state, Brazil, *Rev. bras. meteorol.*, 26(3), 419–432,
817 <https://doi.org/10.1590/S0102-77862011000300008>, 2011.
- 818 Brito, J., Rizzo, L. V., Herckes, P., Vasconcellos, P. C., Caumo, S. E. S., Fornaro, A., Ynoue, R. Y., Artaxo, P. and Andrade,
819 M. F.: Physical–chemical characterisation of the particulate matter inside two road tunnels in the São Paulo Metropolitan Area,
820 *Atmospheric Chemistry and Physics*, 13(24), 12199–12213, <https://doi.org/10.5194/acp-13-12199-2013>, 2013.



- 821 Brito, J., Carbone, S., A. Monteiro dos Santos, D., Dominutti, P., de Oliveira Alves, N., Rizzo, L. V., Artaxo, P.: Disentangling
822 vehicular emission impact on urban air pollution using ethanol as a tracer. *Scientific Reports*, 8, 10679,
823 <https://doi.org/10.1038/s41598-018-29138-7>, 2018.
- 824 Calvo, A. I., Alves, C., Castro, A., Pont, V., Vicente, A. M. and Fraile, R.: Research on aerosol sources and chemical
825 composition: Past, current and emerging issues, *Atmos. Res.*, 120–121, 1–28, <https://doi.org/10.1016/j.atmosres.2012.09.021>,
826 2013.
- 827 Carbone, S., Saarikoski, S., Frey, A., Reyes, F., Reyes, P., Castillo, M., Gramsch, E., Oyola, P., Jayne, J., Worsnop, D. R. and
828 Hillamo, R.: Chemical characterization of submicron aerosol particles in Santiago de Chile, *Aerosol Air Qual. Res.*, 13(2),
829 462–473, <https://doi.org/10.4209/aaqr.2012.10.0261>, 2013.
- 830 Carvalho, J.S., do Nascimento, R.K.S., J Cintra, J.V.F.R.F., da Rosa, N.L.C., Grosseli, G.M., Fadini, P.S., Urban, R.C.: Source
831 apportionment and health impact assessment of atmospheric particulate matter in the city of São Carlos, Brazil, *Chemosphere*,
832 326, 138450, <https://doi.org/10.1016/j.chemosphere.2023.138450>, 2023.
- 833 Caseiro, A., Marr, I.L., Claeys, M., Kasper-Giebl, A., Puxbaum, H., Pio, C.: Determination of saccharides in atmospheric
834 aerosol using anion-exchange high-performance liquid chromatography and pulsed-ampereometric detection, *J. Chromatogr.*
835 A, 1171, 37–45, <https://doi.org/10.1016/j.chroma.2007.09.038>, 2007.
- 836 Caseiro, A., Bauer, H., Schmidl, C., Pio, C. A. and Puxbaum, H.: Wood burning impact on PM₁₀ in three Austrian regions,
837 *Atmos. Environ.*, 43(13), 2186–2195, <https://doi.org/10.1016/j.atmosenv.2009.01.012>, 2009.
- 838 Castanho, A. D. A. and Artaxo, P.: Wintertime and summertime São Paulo aerosol source apportionment study, *Atmos.*
839 *Environ.*, 35(29), 4889–4902, [https://doi.org/10.1016/S1352-2310\(01\)00357-0](https://doi.org/10.1016/S1352-2310(01)00357-0), 2001.
- 840 Caumo, S., Traub, A., Evans, G. and de Castro Vasconcellos, P.: Health risk assessment in atmosphere near a petrochemical
841 industrial complex: Measuring oxidative potential and oxidative burden, *Atmos. Pollut. Res.*, 13(7), 101457,
842 <https://doi.org/10.1016/j.apr.2022.101457>, 2022.
- 843 Cavalli, F., Viana, M., Yttri, K. E., Genberg, J. and Putaud, J. P.: Toward a standardised thermal-optical protocol for measuring
844 atmospheric organic and elemental carbon: the EUSAAR protocol, *Atmos. Meas. Tech.*, 3(1), 79–89,
845 <https://doi.org/10.5194/amt-3-79-2010>, 2010.
- 846 Cecinato, A.: Polynuclear aromatic hydrocarbons (PAH), benz(a)pyrene (BaPY) and nitrated-PAH (NPAH) in suspended
847 particulate matter. *Ann Chim* 87, 483–496, 1997.
- 848 CETESB: Companhia de Tecnologia do Saneamento Ambiental: Relatório de qualidade do ar no Estado de São Paulo 2014,
849 Report of air quality in the São Paulo State 2014, São Paulo, Brazil, available at: [http://ar.cetesb.sp.gov.br/publicacoes-](http://ar.cetesb.sp.gov.br/publicacoes-relatorios/)
850 [relatorios/](http://ar.cetesb.sp.gov.br/publicacoes-relatorios/) (last access: 1 February 2024), 2015.
- 851 CETESB: Companhia de Tecnologia do Saneamento Ambiental: Relatório de qualidade do ar no Estado de São Paulo 2022,
852 Report of air quality in the São Paulo State 2022, São Paulo, Brazil, available at: [http://ar.cetesb.sp.gov.br/publicacoes-](http://ar.cetesb.sp.gov.br/publicacoes-relatorios/)
853 [relatorios/](http://ar.cetesb.sp.gov.br/publicacoes-relatorios/) (last access: 1 February 2024), 2023.
- 854 CETESB: Proconve – Programa de Controle da Poluição do Ar por Veículos Automotores - Companhia Ambiental do Estado
855 de São Paulo, <https://cetesb.sp.gov.br/veicular/proconve/>, last access: 1 April 2022, 2022.
- 856 Chow, W. S., Liao, K., Huang, X. H. H., Leung, K. F., Lau, A. K. H. and Yu, J. Z.: Measurement report: The 10-year trend of
857 PM_{2.5} major components and source tracers from 2008 to 2017 in an urban site of Hong Kong, China, *Atmospheric Chemistry*
858 *and Physics*, 22(17), 11557–11577, <https://doi.org/10.5194/acp-22-11557-2022>, 2022a.
- 859 Chow, W. S., Huang, X. H. H., Leung, K. F., Huang, L., Wu, X. and Yu, J. Z.: Molecular and elemental marker-based source
860 apportionment of fine particulate matter at six sites in Hong Kong, China., *Sci. Total Environ.*, 813, 152652,
861 <https://doi.org/10.1016/j.scitotenv.2021.152652>, 2022b.
- 862 Cohen, A.J., Brauer, M., Burnett, R., Anderson, H.R., Frostad, J., Estep, K., Balakrishnan, K., Brunekreef, B., Dandona, L.,
863 Dandona, R., Feigin, V., Freedman, G., Hubbell, B., Jobling, A., Kan, H., Knibbs, L., Liu, Y., Martin, R., Morawska, L., Pope,
864 C.A. 3rd, Shin, H., Straif, K., Shaddick, G., Thomas, M., van Dingenen, R., van Donkelaar, A., Vos, T., Murray, C.J.L.,
865 Forouzanfar, M.H.: Estimates and 25-year trends of the global burden of disease attributable to ambient air pollution: an
866 analysis of data from the Global Burden of Diseases Study 2015, *The Lancet*, 389(10082), 1907–1918, 2017. Available at:
867 [https://doi.org/10.1016/S0140-6736\(17\)30505-6](https://doi.org/10.1016/S0140-6736(17)30505-6).
- 868 La Colla, N. S., Botté, S.E., and Marcovecchio, J.E.: Atmospheric particulate pollution in South American megacities.,
869 *Environ. Rev.* 29, 3, <https://doi.org/10.1139/er-2020-0105>, 2021.



- 870 CONAMA: Conselho Nacional de MEio Ambiente - Resolução No. 491, 19 De Novembro de 2018,
871 <http://www2.mma.gov.br/port/conama/legiabre.cfm?codlegi=740>, last access: 12 December 2018, 2018.
- 872 Contini, D., Cesari, D., Conte, M. and Donato, A.: Application of PMF and CMB receptor models for the evaluation of the
873 contribution of a large coal-fired power plant to PM₁₀ concentrations., *Sci. Total Environ.*, 560–561, 131–140,
874 <https://doi.org/10.1016/j.scitotenv.2016.04.031>, 2016.
- 875 Decesari, S., Fuzzi, S., Facchini, M. C., Mircea, M., Emblico, L., Cavalli, F., Maenhaut, W., Chi, X., Schkolnik, G., Falkovich,
876 A., Rudich, Y., Claeys, M., Pashynska, V., Vas, G., Kourtev, I., Vermeylen, R., Hoffer, A., Andreae, M. O., Tagliavini, E.,
877 Moretti, F. and Artaxo, P.: Characterization of the organic composition of aerosols from Rondônia, Brazil, during the LBA-
878 SMOCC 2002 experiment and its representation through model compounds, , <https://doi.org/10.5194/acpd-5-5687-2005>, 2005.
- 879 De La Torre-Roche, R. J., Lee, W.-Y. and Campos-Díaz, S. I.: Soil-borne polycyclic aromatic hydrocarbons in El Paso, Texas:
880 analysis of a potential problem in the United States/Mexico border region., *J. Hazard. Mater.*, 163(2–3), 946–958,
881 <https://doi.org/10.1016/j.jhazmat.2008.07.089>, 2009.
- 882 Draxler, R. and Rolph, G.: HYSPLIT (Hybrid Single-Particle Lagrangian Integrated Trajectory) model, NOAA Air Resour.
883 Lab., Silver Spring, MD., 2003.
- 884 Emygdio, A.P.M., Andrade, M.F., Gonçalves, F.L.T., Engling, G., Zanetti, R.H.S., Kumar, P. Biomarkers as indicators of
885 fungal biomass in the atmosphere of São Paulo, Brazil. *Sci. Total Environ.*, 612, 809–821,
886 <https://doi.org/10.1016/j.scitotenv.2017.08.153>, 2018.
- 887 Faisal, M., Ali, U., Kumar, A., Hazarika, N., Singh, V. and Kumar, M.: Festive fireworks in Delhi: A major source of elemental
888 aerosols established through dispersion normalized PMF in a multiyear study, *Atmos. Environ.*, 323, 120394,
889 <https://doi.org/10.1016/j.atmosenv.2024.120394>, 2024.
- 890 Ferreira da Silva, M., Vicente de Assunção, J., de Fátima Andrade, M. and Pesquero, C. R.: Characterization of metal and
891 trace element contents of particulate matter (PM₁₀) emitted by vehicles running on Brazilian fuels-hydrated ethanol and
892 gasoline with 22% of anhydrous ethanol., *J. Toxicol. Environ. Health Part A*, 73(13–14), 901–909,
893 <https://doi.org/10.1080/15287391003744849>, 2010.
- 894 Fine, P. M., Cass, G. R. and Simoneit, B. R.: Chemical characterization of fine particle emissions from fireplace combustion
895 of woods grown in the northeastern United States., *Environ. Sci. Technol.*, 35(13), 2665–2675,
896 <https://doi.org/10.1021/es001466k>, 2001.
- 897 Fountoukis, C. and Nenes, A.: ISORROPIA II: a computationally efficient thermodynamic equilibrium model for K⁺–Ca²⁺–
898 Mg²⁺–NH₄⁺–Na⁺–SO₄²⁻–NO₃⁻–Cl⁻–H₂O aerosols, *Atmospheric Chemistry and Physics*, 7(17), 4639–4659,
899 <https://doi.org/10.5194/acp-7-4639-2007>, 2007.
- 900 Gioia, S. M. C. L., Babinski, M., Weiss, D. J., Spiro, B., Kerr, A. A. F. S., Veríssimo, T. G., Ruiz, I. and Prates, J. C. M.: An
901 isotopic study of atmospheric lead in a megacity after phasing out of leaded gasoline, *Atmos. Environ.*, 149, 70–83,
902 <https://doi.org/10.1016/j.atmosenv.2016.10.049>, 2017.
- 903 Gómez Peláez, L. M., Santos, J. M., de Almeida Albuquerque, T. T., Reis, N. C., Andreão, W. L. and de Fátima Andrade, M.:
904 Air quality status and trends over large cities in South America, *Environmental Science & Policy*, 114, 422–435,
905 <https://doi.org/10.1016/j.envsci.2020.09.009>, 2020.
- 906 Gonçalves, C., Alves, C., Fernandes, A.P., Monteiro, C., Tarelho, L., Evtyugina, M., Pio, C.: Organic compounds in PM_{2.5}
907 emitted from fireplace and woodstove combustion of typical Portuguese wood species, *Atmos. Environ.*, 45, 4533–4545,
908 <https://doi.org/10.1016/j.atmosenv.2011.05.071>, 2011. Goss, M., Swain, D.L., Abatzoglou, J.T., Sarhadi, A., Kolden, C.A.,
909 Williams, A.P., Diffenbaugh, N. S. Climate change is increasing the likelihood of extreme autumn wildfire conditions across
910 California *Environ. Res. Lett.*, 15, 9, <https://doi.org/10.1088/1748-9326/ab83a7>, 2020.
- 911 Graham, B.: Water-soluble organic compounds in biomass burning aerosols over Amazonia1. Characterization by NMR and
912 GC-MS, *J. Geophys. Res.*, 107(D20), 8047, <https://doi.org/10.1029/2001JD000336>, 2002.
- 913 Guo, S., Hu, M., Wang, Z. B., Slanina, J. and Zhao, Y. L.: Size-resolved aerosol water-soluble ionic compositions in the
914 summer of Beijing: implication of regional secondary formation, *Atmospheric Chemistry and Physics*, 10(3), 947–959,
915 <https://doi.org/10.5194/acp-10-947-2010>, 2010.
- 916 Hall, D., Wu, C.-Y., Hsu, Y.-M., Stormer, J., Engling, G., Capeto, K., Wang, J., Brown, S., Li, H.-W. and Yu, K.-M.: PAHs,
917 carbonyls, VOCs and PM_{2.5} emission factors for pre-harvest burning of Florida sugarcane, *Atmos. Environ.*, 55, 164–172,
918 <https://doi.org/10.1016/j.atmosenv.2012.03.034>, 2012.



- 919 Hetem, I.G., and Andrade, M.F.: Characterization of fine particulate matter emitted from the resuspension of road and
920 pavement dust in the Metropolitan Area of São Paulo, Brazil, *Atmos.*, 7, 31, <https://doi.org/10.3390/atmos7030031>, 2016.
- 921 Huang, X., Liu, Z., Zhang, J., Wen, T., Ji, D. and Wang, Y.: Seasonal variation and secondary formation of size-segregated
922 aerosol water-soluble inorganic ions during pollution episodes in Beijing, *Atmos. Res.*, 168, 70–79,
923 <https://doi.org/10.1016/j.atmosres.2015.08.021>, 2016.
- 924 IAG-USP. Boletim Climatológico Anual da Estação Meteorológica do IAG/USP. Seção Técnica de Serviços Meteorológicos
925 – Instituto de Astronomia, Geofísica e Ciências Atmosféricas da Universidade de São Paulo – vol. 22, 2019, São Paulo,
926 IAG/USP, 2023
- 927 Ianniello, A., Spataro, F., Esposito, G., Allegrini, I., Hu, M., and Zhu, T.: Chemical characteristics of inorganic ammonium
928 salts in PM_{2.5} in the atmosphere of Beijing (China), *Atmos. Chem. Phys.*, 11(21), 10803–10822., <https://doi.org/10.5194/acp-11-10803-2011>, 2011.
- 930 INPE: INPE (Instituto Nacional de Pesquisas Espaciais) – Portal do Monitoramento de Queimadas, available at:
931 <https://queimadas.dgi.inpe.br/queimadas/> (last access: 1 February 2024), 2019.
- 932 Jang, H.-N., Seo, Y.-C., Lee, J.-H., Hwang, K.-W., Yoo, J.-I., Sok, C.-H. and Kim, S.-H.: Formation of fine particles enriched
933 by V and Ni from heavy oil combustion: Anthropogenic sources and drop-tube furnace experiments, *Atmos. Environ.*, 41(5),
934 1053–1063, <https://doi.org/10.1016/j.atmosenv.2006.09.011>, 2007.
- 935 Johnson, G. R., Juwono, A. M., Friend, A. J., Cheung, H.-C., Stelcer, E., Cohen, D., Ayoko, G. A. and Morawska, L.: Relating
936 urban airborne particle concentrations to shipping using carbon based elemental emission ratios, *Atmos. Environ.*, 95, 525–
937 536, <https://doi.org/10.1016/j.atmosenv.2014.07.003>, 2014.
- 938 Jung, J., Lee, S., Kim, H., Kim, D., Lee, H. and Oh, S.: Quantitative determination of the biomass-burning contribution to
939 atmospheric carbonaceous aerosols in Daejeon, Korea, during the rice-harvest period, *Atmos. Environ.*, 89, 642–650,
940 <https://doi.org/10.1016/j.atmosenv.2014.03.010>, 2014.
- 941 Keyte, I.J., Harrison, R.M., and Lammel, G.: Chemical reactivity and long-range transport potential of polycyclic aromatic
942 hydrocarbons – a review, *Chem. Soc. Rev.*, 42, 9333–9391, <https://doi.org/10.1039/C3CS60147A>, 2013.
- 943 Khan, Z. Y., Kettler, J., Khwaja, H. A., Naqvi, I. I., Malik, A. and Stone, E. A.: Organic aerosol characterization and source
944 identification in Karachi, Pakistan, *Aerosol Air Qual. Res.*, 18(10), 2550–2564, <https://doi.org/10.4209/aaqr.2017.12.0579>,
945 2018.
- 946 Kováts, N., Hubai, K., Sainnokhoi, T.-A., Hoffer, A. and Teke, G.: Ecotoxicity testing of airborne particulate matter-
947 comparison of sample preparation techniques for the Vibrio fischeri assay., *Environ. Geochem. Health*, 43(11), 4367–4378,
948 <https://doi.org/10.1007/s10653-021-00927-w>, 2021.
- 949 Kulkarni, P., Chellam, S. and Fraser, M. P.: Lanthanum and lanthanides in atmospheric fine particles and their apportionment
950 to refinery and petrochemical operations in Houston, TX, *Atmos. Environ.*, 40(3), 508–520,
951 <https://doi.org/10.1016/j.atmosenv.2005.09.063>, 2006.
- 952 Kumar, P., de Fatima Andrade, M., Ynoue, R. Y., Fornaro, A., de Freitas, E. D., Martins, J., Martins, L. D., Albuquerque, T.,
953 Zhang, Y. and Morawska, L.: New directions: From biofuels to wood stoves: The modern and ancient air quality challenges
954 in the megacity of São Paulo, *Atmos. Environ.*, 140, 364–369, <https://doi.org/10.1016/j.atmosenv.2016.05.059>, 2016.
- 955 Kumar, S., Aggarwal, S. G., Gupta, P. K. and Kawamura, K.: Investigation of the tracers for plastic-enriched waste burning
956 aerosols, *Atmos. Environ.*, 108, 49–58, <https://doi.org/10.1016/j.atmosenv.2015.02.066>, 2015.
- 957 Kumar, P., Morawska, L., Birmili, W., Paasonen, P., Hu, M., Kulmala, M., Harrison, R. M., Norford, L., and Britter, R.: Ultra
958 fine particles in cities, *Environ. Int.*, 66, 1–10, <https://doi.org/10.1016/j.envint.2014.01.013>, 2014.
- 959 Lang, Y.-H., Li, G., Wang, X.-M., and Peng, P.: Combination of Unmix and PMF receptor model to apportion the potential
960 sources and contributions of PAHs in wetland soils from Jiaozhou Bay, China, *Mar. Pollut. Bull.*, 90, 129–134,
961 <https://doi.org/10.1016/j.marpolbul.2014.11.009>, 2015
- 962 Lee, J. D.: *Concise Inorganic Chemistry*, 5th Edn., Wiley, 1070 pp., 1999.
- 963 Lima, F.D.M. *Quantificação e caracterização físico-química do material particulado fino (MP_{2.5}): queima de biomassa em*
964 *fornos de pizzaria na cidade de São Paulo*. Master thesis - University of São Paulo, 2015.
- 965 Linak, W. P., Miller, C. A., Wood, J. P., Shinagawa, T., Yoo, J.-I., Santoianni, D. A., King, C. J., Wendt, J. O. L. and Seo, Y.-
966 C.: High temperature interactions between residual oil ash and dispersed kaolinite powders, *Aerosol Science and Technology*,



- 967 38(9), 900–913, <https://doi.org/10.1080/027868290500805>, 2004.
- 968 Li, Q.-F., Wang-Li, L., Shah, S. B., Jayanty, R. K. M. and Bloomfield, P.: Ammonia concentrations and modeling of inorganic
969 particulate matter in the vicinity of an egg production facility in Southeastern USA., *Environ. Sci. Pollut. Res. Int.*, 21(6),
970 4675–4685, <https://doi.org/10.1007/s11356-013-2417-z>, 2014.
- 971 Li, W., Ge, P., Chen, M., Tang, J., Cao, M., Cui, Y., Hu, K. and Nie, D.: Tracers from Biomass Burning Emissions and
972 Identification of Biomass Burning, *Atmosphere*, 12(11), 1401, <https://doi.org/10.3390/atmos12111401>, 2021.
- 973 Li, J., Carlson, B.E., Yung, Y.L., Lv, D., Hansen, J., Penner, J.E., Liao, H., Ramaswamy, V., Kahn, R.A., Zhang, P., Dubovik,
974 O., Ding, A., Lacis, A.A., Zhang, L., Dong, Y.: Scattering and absorbing aerosols in the climate system. *Nat. Rev. Earth
975 Environ.* 3, 363–379, <https://doi.org/10.1038/s43017-022-00296-7>, 2022.
- 976 Massimi, L., Simonetti, G., Buiairelli, F., Di Filippo, P., Pomata, D., Riccardi, C., Ristorini, M., Astolfi, M.L., Canepari, S.:
977 Spatial distribution of levoglucosan and alternative biomass burning tracers in atmospheric aerosols, in an urban and industrial
978 hot-spot of Central Italy, *Atmos. Res.*, 239, 104904, <https://doi.org/10.1016/j.atmosres.2020.104904>, 2020.
- 979 Marynowski, L., and Simoneit, B.R.T.: Saccharides in atmospheric particulate and sedimentary organic matter: status overview
980 and future perspectives, *Chemosphere*, 288, 132376, <https://doi.org/10.1016/j.chemosphere.2021.132376>, 2022.
- 981 Mbengue, S., Vodička, P., Komínková, K., Zíková, N., Schwarz, J., Prokeš, R., Suchánková, L., Julaha, K., Ondráček, J.,
982 Holoubek, I. and Ždímal, V.: Different approaches to explore the impact of COVID-19 lockdowns on carbonaceous aerosols
983 at a European rural background site., *Sci. Total Environ.*, 892, 164527, <https://doi.org/10.1016/j.scitotenv.2023.164527>, 2023.
- 984 Mehdi, Y., Hornick, J.-L., Istasse, L. and Dufrasne, I.: Selenium in the environment, metabolism and involvement in body
985 functions., *Molecules*, 18(3), 3292–3311, <https://doi.org/10.3390/molecules18033292>, 2013.
- 986 Meng, J., Li, Z., Zhou, R., Chen, M., Li, Y., Yi, Y., Ding, Z., Li, H., Yan, L., Hou, Z. and Wang, G.: Enhanced photochemical
987 formation of secondary organic aerosols during the COVID-19 lockdown in Northern China., *Sci. Total Environ.*, 758, 143709,
988 <https://doi.org/10.1016/j.scitotenv.2020.143709>, 2021.
- 989 de Miranda, R.M., Lopes, F., do Rosário, N.É., Yamasoe, M.A., Landulfo, E., and Andrade, M.F.: The relationship between
990 aerosol particles chemical composition and optical properties to identify the biomass burning contribution to fine particles
991 concentration: a case study for São Paulo city, Brazil., *Environ. Monit. Assess.* 189, 6, <https://doi.org/10.1007/s10661-016-5659-7>, 2017.
- 993 MME, Ministério de Minas e Energia (Ministry of Mines and Energy - Brazil). National Agency of Petroleum, Natural Gas
994 and Biofuels - Brazilian Statistical Yearbook of Petroleum, Natural Gas and Biofuels, 2023, available at:
995 <https://www.gov.br/anp/pt-br/centrais-de-conteudo/publicacoes/anuario-estatistico/arquivos-anuario-estatistico-2023/anuario-2023.pdf/view>, (last access: 15 January 2024) 2023.
- 997 MME, Ministério de Minas e Energia (Ministry of Mines and Energy - Brazil). National Agency of Petroleum, Natural Gas
998 and Biofuels - RESOLUÇÃO ANP N° 968, DE 30 DE ABRIL DE 2024 (ANP RESOLUTION No. 968, OF APRIL 30, 2024)
999 available at: <https://www.in.gov.br/en/web/dou/-/resolucao-anp-n-968-de-30-de-abril-de-2024-557405632>, (last access: 01
1000 July 2024), 2024.
- 1001 Monteiro dos Santos, D., Rizzo, L. V., Carbone, S., Schlag, P. and Artaxo, P.: Physical and chemical properties of urban
1002 aerosols in São Paulo, Brazil: links between composition and size distribution of submicron particles, *Atmospheric Chemistry
1003 and Physics*, 21(11), 8761–8773, <https://doi.org/10.5194/acp-21-8761-2021>, 2021.
- 1004 Monteiro dos Santos, D. A., Brito, J. F., Godoy, J. M. and Artaxo, P.: Ambient concentrations and insights on organic and
1005 elemental carbon dynamics in São Paulo, Brazil, *Atmos. Environ.*, 144, 226–233,
1006 <https://doi.org/10.1016/j.atmosenv.2016.08.081>, 2016.
- 1007 Norris, G., Duvall, R., Brown, S. and Bai, S.: EPA Positive Matrix Factorization (PMF) 5.0 Fundamentals and User Guide,
1008 2014.
- 1009 Oduber, F., Calvo, A. I., Castro, A., Alves, C., Blanco-Alegre, C., Fernández-González, D., Barata, J., Calzolari, G., Nava, S.,
1010 Lucarelli, F., Nunes, T., Rodríguez, A., Vega-Maray, A. M., Valencia-Barrera, R. M. and Fraile, R.: One-year study of airborne
1011 sugar compounds: Cross-interpretation with other chemical species and meteorological conditions, *Atmos. Res.*, 251, 105417,
1012 <https://doi.org/10.1016/j.atmosres.2020.105417>, 2021.
- 1013 de Oliveira Alves, N., Brito, J., Caumo, S., Arana, A., de Souza Hacon, S., Artaxo, P., Hillamo, R., Teinilä, K., Batistuzzo de
1014 Medeiros, S. R. and de Castro Vasconcellos, P.: Biomass burning in the Amazon region: Aerosol source apportionment and
1015 associated health risk assessment, *Atmos. Environ.*, 120, 277–285, <https://doi.org/10.1016/j.atmosenv.2015.08.059>, 2015.



- 1016 de Oliveira Alves, N., Martins Pereira, G., Di Domenico, M., Costanzo, G., Benevenuto, S., de Oliveira Fonoff, A. M., de
1017 Souza Xavier Costa, N., Ribeiro Júnior, G., Satoru Kajitani, G., Cestari Moreno, N., Fotoran, W., Iannicelli Torres, J., de
1018 Andrade, J. B., Matera Veras, M., Artaxo, P., Menck, C. F. M., de Castro Vasconcellos, P., Saldiva, P.: Inflammation response,
1019 oxidative stress and DNA damage caused by urban air pollution exposure increase in the lack of DNA repair XPC protein,
1020 *Environ. Int.*, 145, 106150, <https://doi.org/10.1016/j.envint.2020.106150>, 2020.
- 1021 Paatero, P. and Hopke, P. K.: Discarding or downweighting high-noise variables in factor analytic models, *Anal. Chim. Acta*,
1022 490(1–2), 277–289, [https://doi.org/10.1016/S0003-2670\(02\)01643-4](https://doi.org/10.1016/S0003-2670(02)01643-4), 2003.
- 1023 Paatero, P. and Tapper, U.: Positive matrix factorization: A non-negative factor model with optimal utilization of error
1024 estimates of data values, *Environmetrics*, 5(2), 111–126, <https://doi.org/10.1002/env.3170050203>, 1994.
- 1025 Pacheco, M. T., Parmigiani, M. M. M., de Fatima Andrade, M., Morawska, L. and Kumar, P.: A review of emissions and
1026 concentrations of particulate matter in the three major metropolitan areas of Brazil, *J. Transp. Health*, 4, 53–72,
1027 <https://doi.org/10.1016/j.jth.2017.01.008>, 2017.
- 1028 Pereira, P. A. de P., Lopes, W. A., Carvalho, L. S., da Rocha, G. O., Carvalho, N. De, Loyola, J., Quiterio, S. L., Escaleira, V.,
1029 Arbilla, G., and de Andrade, J. B.: Atmospheric concentrations and dry deposition fluxes of particulate trace metals in Salvador,
1030 Bahia, Brazil, *Atmos. Environ.*, 41, 7837–7850, <https://doi.org/10.1016/j.atmosenv.2007.06.013>, 2007.
- 1031 Pereira, G. M., De Oliveira Alves, N., Caumo, S. E. S., Soares, S., Teinilä, K., Custódio, D., Hillamo, R., Alves, C. and
1032 Vasconcellos, P. C.: Chemical composition of aerosol in São Paulo, Brazil: influence of the transport of pollutants, *Air Qual.*
1033 *Atmos. Health*, 10(4), 457–468, <https://doi.org/10.1007/s11869-016-0437-9>, 2017a.
- 1034 Pereira, G. M., Teinilä, K., Custódio, D., Gomes Santos, A., Xian, H., Hillamo, R., Alves, C. A., Bittencourt de Andrade, J.,
1035 Olímpio da Rocha, G., Kumar, P., Balasubramanian, R., Andrade, M. de F. and de Castro Vasconcellos, P.: Particulate
1036 pollutants in the Brazilian city of São Paulo: 1-year investigation for the chemical composition and source apportionment,
1037 *Atmospheric Chemistry and Physics*, 17(19), 11943–11969, <https://doi.org/10.5194/acp-17-11943-2017>, 2017b.
- 1038 Pereira, G.M., Oraggio, B., Teinilä, K., Custódio, D., Huang, X., Hillamo, R., Alves, C.A., Balasubramanian, R., Rojas, N.Y.,
1039 Sanchez-Ccoyllo, O.R., and Vasconcellos, P.C.: A comparative chemical study of PM₁₀ in three Latin American cities: Lima,
1040 Medellín, and São Paulo. *Air Qual. Atmos. Health*, 12, 1141–1152, <https://doi.org/10.1007/s11869-019-00735-3>, 2019.
- 1041 Pereira, G. M., da Silva Caumo, S. E., Grandis, A., do Nascimento, E. Q. M., Correia, A. L., de Melo Jorge Barbosa, H.,
1042 Marcondes, M. A., Buckeridge, M. S. and de Castro Vasconcellos, P.: Physical and chemical characterization of the 2019
1043 “black rain” event in the Metropolitan Area of São Paulo, Brazil, *Atmos. Environ.*, 248, 118229,
1044 <https://doi.org/10.1016/j.atmosenv.2021.118229>, 2021.
- 1045 Pereira, G. M., Kamigauti, L. Y., Nogueira, T., Gavidia-Calderón, M. E., Monteiro Dos Santos, D., Evtuygina, M., Alves, C.,
1046 Vasconcellos, P. de C., Freitas, E. D. and Andrade, M. de F.: Emission factors for a biofuel impacted fleet in South America’s
1047 largest metropolitan area., *Environ. Pollut.*, 331(Pt 2), 121826, <https://doi.org/10.1016/j.envpol.2023.121826>, 2023a.
- 1048 Pereira, G. M., Nogueira, T., Kamigauti, L. Y., Monteiro Dos Santos, D., Nascimento, E. Q. M., Martins, J. V., Vicente, A.,
1049 Artaxo, P., Alves, C., de Castro Vasconcellos, P. and de Fatima Andrade, M.: Particulate matter fingerprints in biofuel
1050 impacted tunnels in South America’s largest metropolitan area., *Sci. Total Environ.*, 856(Pt 2), 159006,
1051 <https://doi.org/10.1016/j.scitotenv.2022.159006>, 2023b.
- 1052 Pio, C. A., Legrand, M., Oliveira, T., Afonso, J., Santos, C., Caseiro, A., Fialho, P., Barata, F., Puxbaum, H., Sanchez-Ochoa,
1053 A., Kasper-Giebl, A., Gelencsér, A., Preunkert, S. and Schock, M.: Climatology of aerosol composition (organic versus
1054 inorganic) at nonurban sites on a west-east transect across Europe, *J. Geophys. Res.*, 112(D23),
1055 <https://doi.org/10.1029/2006JD008038>, 2007.
- 1056 Pöschl, U.: Atmospheric aerosols: composition, transformation, climate and health effects., *Angew. Chem. Int. Ed.*, 44(46),
1057 7520–7540, <https://doi.org/10.1002/anie.200501122>, 2005.
- 1058 Ravindra, K., Sokhi, R. and Vangrieken, R.: Atmospheric polycyclic aromatic hydrocarbons: Source attribution, emission
1059 factors and regulation, *Atmos. Environ.*, 42(13), 2895–2921, <https://doi.org/10.1016/j.atmosenv.2007.12.010>, 2008.
- 1060 Ribeiro, F.N.D., de Oliveira, A.P., Soares, J., de Miranda, R.M., Barlage, M., Chen, F.: Effect of sea breeze propagation on
1061 the urban boundary layer of the metropolitan region of Sao Paulo, Brazil, *Atmos. Res.* 214, 174–188,
1062 <https://doi.org/10.1016/j.atmosres.2018.07.015>, 2018.
- 1063 Sánchez-Ccoyllo, O. R. and de, F.: The influence of meteorological conditions on the behavior of pollutants concentrations in
1064 São Paulo, Brazil., *Environ. Pollut.*, 116(2), 257–263, [https://doi.org/10.1016/s0269-7491\(01\)00129-4](https://doi.org/10.1016/s0269-7491(01)00129-4), 2002.



- 1065 Santos, T. C. dos, Reboita, M. S. and Carvalho, V. S. B.: Investigação da Relação entre Variáveis Atmosféricas e a
1066 Concentração de PM_{10} E O_3 no Estado de São Paulo, *Rev. Bras. Meteorol.*, 33(4), 631–645, <https://doi.org/10.1590/0102-7786334006>, 2018.
- 1068 Satsangi, A., Mangal, A., Agarwal, A., Lakhani, A., and Kumari, K. M.: Variation of carbonaceous aerosols and water soluble
1069 inorganic ions during winter haze in two consecutive years. *Atmos. Pollut. Res.*, 12(3), 242–251,
1070 <https://doi.org/10.1016/j.apr.2020.12.011>, 2021.
- 1071 Scaramboni, C. Impacto da queima de biomassa na concentração de compostos policíclicos aromáticos e na toxicidade *in vitro*
1072 do material particulado atmosférico de Ribeirão Preto-SP. Doctoral thesis - University of São Paulo, 2023.
- 1073 Schraufnagel, D. E.: The health effects of ultrafine particles., *Exp. Mol. Med.*, 52(3), 311–317, <https://doi.org/10.1038/s12276-020-0403-3>, 2020.
- 1075 SEADE, Fundação Sistema Estadual de Análise de Dados - São Paulo State Data Analysis System Foundation, available at:
1076 https://www.seade.gov.br/wp-content/uploads/2021/09/MapaIndustria_abril2019.pdf, (last access: 15 January 2024), 2019.
- 1077 Serafeim, E., Besis, A., Kouras, A., Farias, C. N., Yera, A. B., Pereira, G. M., Samara, C. and de Castro Vasconcellos, P.:
1078 Oxidative potential of ambient $PM_{2.5}$ from São Paulo, Brazil: Variations, associations with chemical components and source
1079 apportionment, *Atmos. Environ.*, 298, 119593, <https://doi.org/10.1016/j.atmosenv.2023.119593>, 2023.
- 1080 Shen, H., Tao, S., Wang, R., Wang, B., Shen, G., Li, W., Su, S., Huang, Y., Wang, X., Liu, W., Li, B. and Sun, K.: Global
1081 time trends in PAH emissions from motor vehicles., *Atmos. Environ.*, 45(12), <https://doi.org/10.1016/j.atmosenv.2011.01.054>,
1082 2011.
- 1083 Simoneit, B. R. T.: Biomass burning — a review of organic tracers for smoke from incomplete combustion, *Applied*
1084 *Geochemistry*, 17(3), 129–162, [https://doi.org/10.1016/S0883-2927\(01\)00061-0](https://doi.org/10.1016/S0883-2927(01)00061-0), 2002.
- 1085 Souto-Oliveira, C. E., Babinski, M., Araújo, D.F., and Andrade, M.F.: Multi-isotopic fingerprints (Pb, Zn, Cu) applied for
1086 urban aerosol source apportionment and discrimination, *Sci. Total Environ.*, 626, 1350-1366,
1087 <https://doi.org/10.1016/j.scitotenv.2018.01.192>, 2018.
- 1088 Souto-Oliveira, C. E., Kamigauti, L. Y., Andrade, M. F., and Babinski, M.: Improving Source Apportionment of Urban Aerosol
1089 Using Multi-Isotopic Fingerprints (MIF) and Positive Matrix Factorization (PMF): Cross-Validation and New Insights. *Front.*
1090 *Environ. Sci.* 9, 623915, <https://doi.org/10.3389/fenvs.2021.623915>, 2021.
- 1091 Souto-Oliveira, C. E., Marques, M. T. A., Nogueira, T., Lopes, F. J. S., Medeiros, J. A. G., Medeiros, I. M. M. A., Moreira,
1092 G. A., da Silva Dias, P. L., Landulfo, E. and Andrade, M. de F.: Impact of extreme wildfires from the Brazilian Forests and
1093 sugarcane burning on the air quality of the biggest megacity on South America., *Sci. Total Environ.*, 888, 163439,
1094 <https://doi.org/10.1016/j.scitotenv.2023.163439>, 2023.
- 1095 Souza, D. Z., Vasconcellos, P. C., Lee, H., Aurela, M., Saarnio, K., Teinilä, K. and Hillamo, R.: Composition of $PM_{2.5}$ and
1096 PM_{10} collected at urban sites in Brazil, *Aerosol Air Qual. Res.*, 14(1), 168–176, <https://doi.org/10.4209/aaqr.2013.03.0071>,
1097 2014.
- 1098 Sun, J., Shen, Z., Zhang, Y., Zhang, Q., Lei, Y., Huang, Y., Niu, X., Xu, H., Cao, J., Ho, S.S.H. and Li, X.: Characterization
1099 of $PM_{2.5}$ source profiles from typical biomass burning of maize straw, wheat straw, wood branch, and their processed products
1100 (briquette and charcoal) in China, *Atmos. Environ.* 205, 36–45, <https://doi.org/10.1016/j.atmosenv.2019.02.038>, 2019.
- 1101 Tang, X., Zhang, X., Ci, Z., Guo, J. and Wang, J.: Speciation of the major inorganic salts in atmospheric aerosols of Beijing,
1102 China: Measurements and comparison with model, *Atmos. Environ.*, 133, 123–134,
1103 <https://doi.org/10.1016/j.atmosenv.2016.03.013>, 2016.
- 1104 Thorpe, A. and Harrison, R. M.: Sources and properties of non-exhaust particulate matter from road traffic: A review, *Sci.*
1105 *Total Environ.*, 400(1–3), 270–282, <https://doi.org/10.1016/j.scitotenv.2008.06.007>, 2008.
- 1106 Tobiszewski, M. and Namieśnik, J.: PAH diagnostic ratios for the identification of pollution emission sources., *Environ.*
1107 *Pollut.*, 162, 110–119, <https://doi.org/10.1016/j.envpol.2011.10.025>, 2012.
- 1108 Turpin, B.J., Lim, H.: Species contributions to $PM_{2.5}$ mass concentrations: revisiting common assumptions for estimating
1109 organic mass, *Aerosol Sci. Technol.*, 35, 602-610, 2001.
- 1110 Urban, R. C., Lima-Souza, M., Caetano-Silva, L., Queiroz, M. E. C., Nogueira, R. F. P., Allen, A. G., Cardoso, A. A., Held,
1111 G. and Campos, M. L. A. M.: Use of levoglucosan, potassium, and water-soluble organic carbon to characterize the origins of
1112 biomass-burning aerosols, *Atmos. Environ.*, 61, 562–569, <https://doi.org/10.1016/j.atmosenv.2012.07.082>, 2012.
- 1113 Urban, R. C., Alves, C. A., Allen, A. G., Cardoso, A. A., Queiroz, M. E. C. and Campos, M. L. A. M.: Sugar markers in aerosol



- 1114 particles from an agro-industrial region in Brazil, *Atmos. Environ.*, 90, 106–112,
1115 <https://doi.org/10.1016/j.atmosenv.2014.03.034>, 2014.
- 1116 Valente, F. and Laurini, M.: Pre-harvest sugarcane burning: A statistical analysis of the environmental impacts of a regulatory
1117 change in the energy sector, *Cleaner Engineering and Technology*, 4, 100255, <https://doi.org/10.1016/j.clet.2021.100255>,
1118 2021.
- 1119 Vara-Vela, A., Andrade, M. F., Kumar, P., Ynoue, R. Y. and Muñoz, A. G.: Impact of vehicular emissions on the formation
1120 of fine particles in the Sao Paulo Metropolitan Area: a numerical study with the WRF-Chem model, *Atmospheric Chemistry
1121 and Physics*, 16(2), 777–797, <https://doi.org/10.5194/acp-16-777-2016>, 2016.
- 1122 Vasconcellos, P. C., Souza, D. Z., Sanchez-Ccoyllo, O., Bustillos, J. O. V., Lee, H., Santos, F. C., Nascimento, K. H., Araújo,
1123 M. P., Saarnio, K., Teinilä, K., and Hillamo, R.: Determination of anthropogenic and biogenic compounds on atmospheric
1124 aerosol collected in urban, biomass burning and forest areas in São Paulo, Brazil, *Sci. Total Environ.*, 408, 5836–5844,
1125 <https://doi.org/10.1016/j.scitotenv.2010.08.012>, 2010.
- 1126 Vieira-Filho, M. S., Ito, D. T., Pedrotti, J. J., Coelho, L. H. G. and Fornaro, A.: Gas-phase ammonia and water-soluble ions in
1127 particulate matter analysis in an urban vehicular tunnel., *Environ. Sci. Pollut. Res. Int.*, 23(19), 19876–19886,
1128 <https://doi.org/10.1007/s11356-016-7177-0>, 2016a.
- 1129 Vieira-Filho, M.S., Pedrotti, J. J., and Fornaro, A.: Water-soluble ions species of size-resolved aerosols: Implications for the
1130 atmospheric acidity in São Paulo megacity, Brazil, *Atmos. Res.*, 181, 281–287,
1131 <https://doi.org/10.1016/j.atmosres.2016.07.006>, 2016b.
- 1132 Vieira, E. V. R., do Rosario, N. E., Yamasoe, M. A., Morais, F. G., Martinez, P. J. P., Landulfo, E. and Maura de Miranda, R.:
1133 Chemical characterization and optical properties of the aerosol in São Paulo, Brazil, *Atmosphere*, 14(9), 1460,
1134 <https://doi.org/10.3390/atmos14091460>, 2023.
- 1135 Watson, J.G., Chow, J.C., Houck, J.E.: PM_{2.5} chemical source profiles for vehicle exhaust, vegetative burning, geological
1136 material, and coal burning in Northwestern Colorado during 1995, *Chemosphere*, 43, 1141–1151,
1137 [https://doi.org/10.1016/S0045-6535\(00\)00171-5](https://doi.org/10.1016/S0045-6535(00)00171-5), 2001.
- 1138 WHO, World Health Organization: WHO global air quality guidelines: Particulate matter (PM_{2.5} and PM₁₀), ozone, nitrogen
1139 dioxide, sulfur dioxide and carbon monoxide, Geneva., 2021.
- 1140 Wu, X., Vu, T. V., Shi, Z., Harrison, R. M., Liu, D. and Cen, K.: Characterization and source apportionment of carbonaceous
1141 PM_{2.5} particles in China - A review, *Atmos. Environ.*, 189, 187–212, <https://doi.org/10.1016/j.atmosenv.2018.06.025>, 2018.
- 1142 Yamagami, M., Ikemori, F., Nakashima, H., Hisatsune, K. and Osada, K.: Decreasing trend of elemental carbon concentration
1143 with changes in major sources at Mega city Nagoya, Central Japan, *Atmos. Environ.*, 199, 155–163,
1144 <https://doi.org/10.1016/j.atmosenv.2018.11.014>, 2019.
- 1145 Yassaa, N., Meklati, B. Y., Cecinato, A., and Marino, F.: Organic aerosols in urban and waste landfill of Algiers metropolitan
1146 area: occurrence and sources, *Environ. Sci. Technol.* 35, 306–311, <https://doi.org/10.1021/es991316d>, 2001.
- 1147 Yunker, M. B., Macdonald, R. W., Vingarzan, R., Mitchell, R. H., Goyette, D. and Sylvestre, S.: PAHs in the Fraser River
1148 basin: a critical appraisal of PAH ratios as indicators of PAH source and composition, *Org. Geochem.*, 33(4), 489–515,
1149 [https://doi.org/10.1016/S0146-6380\(02\)00002-5](https://doi.org/10.1016/S0146-6380(02)00002-5), 2002.
- 1150 Yu, J. Z., Xu, J. and Yang, H.: Charring characteristics of atmospheric organic particulate matter in thermal analysis., *Environ.
1151 Sci. Technol.*, 36(4), 754–761, <https://doi.org/10.1021/es015540q>, 2002.
- 1152 Yuan, H., Zhuang, G., Li, J., Wang, Z., Li, J.: Mixing of mineral with pollution aerosols in dust season in Beijing: Revealed
1153 by source apportionment study, *Atmo. Environ.* 42, 2141–2157, ISSN 1352-2310,
1154 <https://doi.org/10.1016/j.atmosenv.2007.11.048>, 2008.
- 1155 Zhang, W., Zhang, S., Wan, C., Yue, D., Ye, Y. and Wang, X.: Source diagnostics of polycyclic aromatic hydrocarbons in
1156 urban road runoff, dust, rain and canopy throughfall., *Environ. Pollut.*, 153(3), 594–601,
1157 <https://doi.org/10.1016/j.envpol.2007.09.004>, 2008.
- 1158 Zhu, C.-S., Cao, J.-J., Tsai, C.-J., Shen, Z.-X., Han, Y.-M., Liu, S.-X. and Zhao, Z.-Z.: Comparison and implications of PM_{2.5}
1159 carbon fractions in different environments., *Sci. Total Environ.*, 466–467, 203–209,
1160 <https://doi.org/10.1016/j.scitotenv.2013.07.029>, 2014.
- 1161 Zhu, C., Kawamura, K. and Kunwar, B.: Effect of biomass burning over the western North Pacific Rim: wintertime maxima
1162 of anhydrosugars in ambient aerosols from Okinawa, *Atmospheric Chemistry and Physics*, 15(4), 1959–1973,

<https://doi.org/10.5194/egusphere-2024-2212>

Preprint. Discussion started: 23 August 2024

© Author(s) 2024. CC BY 4.0 License.



1163 <https://doi.org/10.5194/acp-15-1959-2015>, 2015.